Lie sphere geometry in lattice cosmology

Michael Fennen[1] and Domenico Giulini[1,2]

[1] Center for Applied Space Technology and Microgravity, University of Bremen, Bremen, Germany
[2] Institute for Theoretical Physics, Leibniz University of Hannover, Hannover, Germany

E-mail: giulini@itp.uni-hannover.de

Abstract

In this paper we propose to use *Lie sphere geometry* as a new tool to systematically construct time-symmetric initial data for a wide variety of generalised black-hole configurations in lattice cosmology. These configurations are iteratively constructed analytically and may have any degree of geometric irregularity. We show that for negligible amounts of dust these solutions are similar to the swiss-cheese models at the moment of maximal expansion. As Lie sphere geometry has so far not received much attention in cosmology, we will devote a large part of this paper to explain its geometric background in a language familiar to general relativists.

Keywords: inhomogeneous cosmology, black holes, Lie sphere geometry

(Some figures may appear in colour only in the online journal)

1. Introduction

In their seminal paper [37] of 1957, Richard Lindquist and John Wheeler introduced the idea to approximate the global dynamics of homogeneous and isotropic cosmological models by lattice-like configurations of vacuum Schwarzschild geometries. Approximate homogeneity and isotropy was translated into the requirement that this lattice should be a regular one, such that each lattice site is equally distant to its nearest neighbours. Hence, approximating a round 3-sphere, which for the moment we think of as embedded into Euclidean $\mathbb{R}^4$, this implies that the lattice sites are given by the vertices of inscribed 4-dimensional regular convex polytopes (platonic solids), of which there are six in four dimensions, corresponding to $N = 5, 8, 16, 24, 120$ and 600 vertices.

In order to avoid confusion, the method of lattice cosmology has to be clearly distinguished from the related but different so-called 'swiss-cheese' models, which we shall briefly describe

and which also play some role in this paper. The swiss-cheese models are constructed from the homogeneous and isotropic models in standard dust-matter cosmology by introducing local inhomogeneities as follows: replace the spherically-symmetric and locally homogeneous geometry in a neighbourhood of a vertex (the method works for any point, but in order to compare it with lattice cosmology we stick to the vertices) by the spherically-symmetric and locally inhomogeneous vacuum Schwarzschild geometry with appropriate matching conditions at the boundary to the dust-filled complement. The matching conditions require the metric to be continuously differentiable across the boundary and essentially impose the condition that the mass of the black-hole equals that of the removed dust (they must be strictly equal in terms of the Misner–Sharp mass; compare [12]). This works for any sizes of balls centred around each vertex, as long as the collection of balls have no pairwise intersections. Outside the balls the dust is still present and the local geometry is still that of the round 3-sphere (in case of positive curvature, to which we restrict attention here). As already stated, inside the balls the geometry is strictly spherically symmetric, even though the distribution of black-holes around them on neighbouring vertices is only approximately so. This is because the remaining dust just enforces this symmetry by construction. It should be intuitively obvious why these are referred to as 'swiss-cheese' models.

In contrast, in lattice cosmology, *all* the dust is replaced by a finite number of black-holes, none of which will now give rise to a strictly spherically symmetric geometry in its neighbourhood. Approximate spherical symmetry will be improved by increasing the number of black-holes, i.e. the number of vertices, but never attained exactly. There is now no matter present whatsoever and all gravitating masses are concentrated in black-holes. Hence the evolution equations are pure vacuum.

Now, the central ideas behind lattice cosmology is that *as regards certain aspects of the overall gravitational dynamics, we may replace all matter by an appropriate but fictitious distributions of black holes*. The hope connected with this strategy is to gain reliable analytical insight into various aspects of global gravitational dynamics in cosmology, like, e.g. the backreaction and fitting problems [14]. This hope rests on the fact that now we are dealing with the *vacuum* Einstein equations and its associated initial-value problem, the analytic treatment of which, albeit still complicated, is considerably simpler than that of the coupled Einstein-matter equations for realistic models of matter. Moreover, the particular non-linear form of Einstein's vacuum equations can lead to a characteristic enhancements of backreaction from multiscale configurations that one would like to study in isolation and unaffected by possible stress–energy artefacts of matter; compare [11, 33] for very lucid discussions of this point.

In fact, for special classes of initial data the matter-free constraint equations assume a linear form, so as to allow for the possibility to simply add solutions. This linearity will be essential to the method used here. We refer to [5] for a recent comprehensive review of the expectations and achievements connected with lattice cosmology. More specifically, we refer to [10, 15] for general introductions and lucid discussion of the backreaction problem, once more to [11, 33] for very illuminating discussions concerning the impact of general relativity's non-linearity for backreaction, to [17] and again to [33] for the question of how to quantify backreaction, to [38] for an extensive study of redshifts and integrated Sachs–Wolfe effects, and [6] for a general discussion of light-propagation in lattice cosmology.

In this paper we shall concentrate on the problem of how to analytically construct suitable multi black-hole initial data, leaving the all-important problem of their evolution aside for the time being. The familiar situation in the Cauchy problem of general relativity is that careful analytical work is invested in the construction of initial data in order to map the envisaged physical situation in an explicit, well controlled, and interpretable fashion, but that the evolution of these data has to be left to the computer [3]. In the present context of lattice

cosmology, first steps in numerical evolution were taken in [4] considering data for a regular lattice of eight black-holes.

Moreover, also for regular lattices, it has been argued in [16] that the resulting local discrete rotation and reflection symmetries suffice to render the Einstein evolution equations ordinary (rather than partial) differential equations for points in the one-dimensional fixed-point set of these symmetries, thus effectively decoupling the evolution of the geometry at these points from that of their spatial neighbours. If this were true, long term predictions for the geometry of these lower-dimensional structures could indeed be made, as claimed in [16]. However, this claim has subsequently been scrutinised numerically and analytically on the basis of Einstein's evolution equations in [34] and found to be in error on both accounts. The error was shown to be due to the actual existence of a term containing second spatial derivatives of the metric which is nevertheless compatible with the local discrete symmetries (and hence had been erroneously excluded *a priori* in [16]).

In [37] and its follow-up papers, the requirement of regularity of the lattice formed by the sites of the black-holes was explicitly imposed. A first relaxation from strict regularity was considered in [18] in relation to structure formation and backreaction. Their generalisation still started from one of the six regular lattices, but then allowed to 'explode' each black-hole into a cluster of other black-holes in a special way that maintains overall statistical homogeneity and isotropy. Our method presented in this paper can be seen as a significant generalisation of theirs, resting on a novel application of Lie sphere geometry, that so far does not seem to have enjoyed any application to cosmological model-building whatsoever. The method itself, the foundations of which we shall explain in the next section, is certainly very powerful, though the extent to which it may profitably applied in cosmology remains to be seen. As an illustrative example, we include a comparison between special black-hole configurations that we called 'unifoamy' in lattice- and swiss-cheese cosmology. This paper is based in parts on [22].

2. Lie sphere geometry and Apollonian packings

In this section we wish to acquaint the reader with the geometric ideas behind *Lie sphere geometry* and its power to study and construct configurations of (round) spheres isometrically embedded in Riemannian manifolds of constant-curvature. As the name suggests, the geometric ideas were first introduced by Sophus Lie (1842–1899), in fact in his doctoral thesis [36]. Our presentation will follow modern terminology and notation. As already stressed, this geometric method has—quite surprisingly and to the best of our knowledge—not been employed in the general-relativistic initial-value problem and hardly ever in astrophysics and cosmology. The only two notable exceptions we are aware of concern the statistics of craters on planetary bodies [24] and the statistics of cosmological voids [25][3]. In our paper we will use it to systematically construct initial data for Einstein's field equations applied to lattice cosmology.

Let us now explain in some more detail those aspects of Lie sphere geometry that are of interest to us and which we reformulate and amend according to our needs. A standard mathematical textbook on Lie sphere geometry is by Cecil [13], which contains much—but not all—of what we say in its first chapters. The central object in Lie sphere geometry is the configuration space of spheres which, as we will see discuss in detail, turns out to be an old friend of all relativists.

---

[3] We thank Marcus Werner for pointing out these references.

2.1. DeSitter space as configuration space for spherical caps, or oriented hyperspheres, within spheres

Throughout we often consider the real vector space $\mathbb{R}^{n+1}$ together with its Euclidean canonical inner product. Elements in $\mathbb{R}^{n+1}$ are denoted by bold-faced letters, like $\boldsymbol{X}$ and $\boldsymbol{P}$, and their inner product $\boldsymbol{X} \cdot \boldsymbol{P}$ is defined as usual. The inner product defines a norm $\|\boldsymbol{X}\| := \sqrt{\boldsymbol{X} \cdot \boldsymbol{X}}$. The n-sphere of unit-norm vectors in $\mathbb{R}^{n+1}$ is

$$S^n = \left\{ \boldsymbol{X} \in \mathbb{R}^{n+1} : \|\boldsymbol{X}\| = 1 \right\}. \tag{1}$$

The geodesic distance $\Lambda(\boldsymbol{X}, \boldsymbol{P}) \in [0, \pi]$ between the two points $\boldsymbol{X}$ and $\boldsymbol{P}$ on S^n is given by

$$\Lambda(\boldsymbol{X}, \boldsymbol{P}) := \arccos(\boldsymbol{X} \cdot \boldsymbol{P}). \tag{2}$$

A *spherical α-cap* on S^n, with $\alpha \in (0, \pi)$, centered at $\boldsymbol{P} \subset S^n$ is the set of all points $\boldsymbol{X} \in S^n$ whose geodesic distance from $\boldsymbol{P}$ is less or equal to α. Hence these points satisfy

$$\boldsymbol{X} \cdot \boldsymbol{P} \geqslant \cos \alpha. \tag{3}$$

It should be read as an equation describing the intersection between the half-space $\{\boldsymbol{X} \in \mathbb{R}^{n+1} : \boldsymbol{X} \cdot \boldsymbol{P} \geqslant \cos \alpha\}$ with S^n. See figure 1 for an illustration of the cases $n = 1, 2$.

Now, the central idea of Lie sphere geometry is to regard S^n not as subset of $\mathbb{R}^{n+1}$ endowed with the Euclidean inner product, but rather as subset of $(n + 2)$-dimensional Minkowski space $\mathbb{R}^{1,n+1}$, i.e. the vector space $\mathbb{R}^{n+2}$ endowed with a non-degenerate symmetric bilinear form of signature $(1, n + 1)$, the so-called Minkowski metric or Minkowski inner product, which in the 'mostly-plus-convention' that we shall use here is given by

$$\langle \boldsymbol{\xi}_1, \boldsymbol{\xi}_2 \rangle := -\xi_1^0 \xi_2^0 + \sum_{a=1}^{n+1} \xi_1^a \xi_2^a. \tag{4}$$

Hence spacelike vectors have positive and timelike vectors have negative Minkowski square.

The embedding of $S^n \subset \mathbb{R}^{n+1}$ into $\mathbb{R}^{1,n+1}$ is then given by regarding $\mathbb{R}^{n+1}$ as affine spacelike hyperplane of constant time (first coordinate in $\mathbb{R}^{1,n+1}$) equal to 1. Then

$$\mathbb{R}^{n+1} \supset S^n \ni \boldsymbol{X} \longmapsto \boldsymbol{\xi} := (1, \boldsymbol{X}) \in \mathbb{R}^{1,n+1}. \tag{5}$$

Obviously $\langle \boldsymbol{\xi}, \boldsymbol{\xi} \rangle = 0$, so that $S^n \subset \mathbb{R}^{1,n+1}$ is the intersection of the constant-time hyperplane with the future light-cone with vertex at the origin. This intersection is also called the *Möbius sphere*.

Like above, a spherical cap on the Möbius sphere can be obtained by intersecting the latter with a half space. But now the half space is such that its boundary hyperplane, which is timelike, contains the origin of $\mathbb{R}^{1,n+1}$. Hence we can rewrite equation (3) as

$$\langle \boldsymbol{\xi}, \boldsymbol{\omega} \rangle \geqslant 0, \tag{6}$$

where (recall $\csc(x) = 1/\sin(x)$)

$$\boldsymbol{\omega} = (\cot(\alpha), \boldsymbol{P} \csc(\alpha)) \tag{7}$$

is a normalized spacelike vector, i.e. $\langle \boldsymbol{\omega}, \boldsymbol{\omega} \rangle = 1$, which is Minkowski-perpendicular to the boundary hyperplane of the half-space and oriented such that it points into the interior of the half-space. It is sometimes referred to as *Lie (sphere) vector*. It establishes a bijection between the set of spherical caps of non-zero radius in S^n—equivalently the set of oriented $(n-1)$ spheres (hyperspheres) of non-zero radius in S^n—and the set of unit spacelike vectors in $\mathbb{R}^{1,n+1}$. The latter is just the one-sheeted timelike unit hyperboloid in $(n + 2)$-dimensional Minkowski space, known to relativists as $(n + 1)$-dimensional de Sitter space of unit radius,
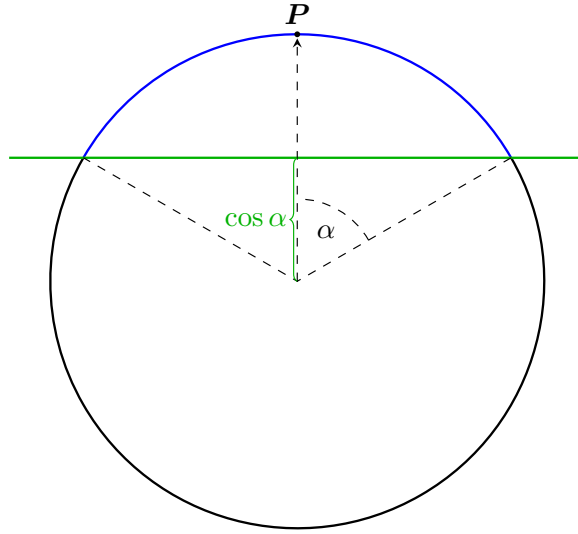
Figure 1. Spherical cap in $n = 1$ dimensions with centre $\boldsymbol{P}$ and radius α. The $n = 2$ case is obtained by rotating the figure about the vertical symmetry axis.

which we denote by dS^{n+1}. It thus assumes the role of the configuration space of spherical caps—or oriented hyperspheres—in S^n. Remarkably, this configuration space is itself endowed with a natural *Lorentzian* geometry that it inherits from being imbedded into Minkowski space and that is well known to relativists. Indeed, if we restrict the $(1, n + 1)$ Minkowski metric

$$\boldsymbol{\eta} = -\mathbf{d}\omega^0 \otimes \mathbf{d}\omega^0 + \sum_{a=1}^{n+1} \mathbf{d}\omega^a \otimes \mathbf{d}\omega^a \tag{8}$$

to the tangent bundle of the embedded timelike hyperboloid in the parametrisation (7), where $\boldsymbol{P}$ is normalised, so that $\boldsymbol{P} \cdot \mathbf{d}\boldsymbol{P} = 0$, we immediately get

$$\boldsymbol{g}^{\mathrm{dS}^{(n+1)}} = \csc^2(\alpha)\left(-\mathbf{d}\alpha \otimes \mathbf{d}\alpha + \boldsymbol{g}^{S^n}\right). \tag{9}$$

Here $\boldsymbol{g}^{S^n}$ denotes the standard round metric of the unit n-sphere S^n given by restricting $\sum_{i=1}^{n+1} \mathbf{d}P_i \otimes \mathbf{d}P_i =: \mathbf{d}\boldsymbol{P}\dot{\otimes}\mathbf{d}\boldsymbol{P}$ to the n-sphere $\|\boldsymbol{P}\| = 1$. Replacing $\alpha \in (0, \pi)$ by $t \in (-\infty, \infty)$ according to the reparametrisation

$$t = t(\alpha) := \begin{cases} -\mathrm{arccosh}\big(\csc(\alpha)\big) & \text{for} \quad 0 < \alpha \leqslant \pi/2 \\ +\mathrm{arccosh}\big(\csc(\alpha)\big) & \text{for} \quad \pi/2 \leqslant \alpha < \pi \end{cases} \tag{10}$$

leads to the well known form of the deSitter metric used for $n = 3$ in standard relativistic cosmology:

$$\boldsymbol{g}^{\mathrm{dS}^{(n+1)}} = -\mathbf{d}t \otimes \mathbf{d}t + \cosh^2(t)\boldsymbol{g}^{S^n}. \tag{11}$$

Note that the function on the right-hand side of (10) maps the interval $(0, \pi)$ strictly increasing and differentiably onto $(-\infty, \infty)$. Indeed, the derivative of $t(\alpha)$ is just $t'(\alpha) = \csc(\alpha)$ for all $0 < \alpha < \pi$.

In this fashion the set of spherical caps in S^n is not only put into bijective correspondence with points in dS^{n+1}, but is also endowed with the structure of a maximally symmetric

Lorentzian manifold with metric $\boldsymbol{g}^{\mathrm{dS}^{(n+1)}}$, the geometry of which turns out to be very useful indeed, with many and sometimes surprising applications. For example, in $n = 2$ and $n = 3$ dimensions, the volume form induced by this metric has been used for statistical discussions of distributions of planetary craters in [24] and cosmic voids in [25], respectively. In figure 2 we illustrate once more the geometric objects underlying this bijective correspondence between spherical caps of—or oriented hyperspheres in—the Möbius sphere S^n and deSitter space $\mathrm{dS}^{(n+1)}$ in the case $n = 1$.

As regards the Lorentzian signature of $\boldsymbol{g}^{\mathrm{dS}^{(n+1)}}$, note that changing the location of the spherical cap's centre while keeping the radius fixed corresponds to a spacelike motion in configuration space, while a change in radius with fixed centre corresponds to a timelike motion. Increasing cap radii correspond to increasing α and hence increasing t according to (10). The set of caps carries a natural partial-order relation given by inclusion. It is geometrically obvious that a cap with centre $\boldsymbol{P}$ and geodesic radius α is properly included in another one parametrised by $\boldsymbol{P}'$ and α', if and only if the geodesic distance between the centres is less than, or equal to, the difference $\alpha' - \alpha$ of their geodesic radii. As the geodesic distance between $\boldsymbol{P}$ and $\boldsymbol{P}'$ is measured by $\boldsymbol{g}^{S^n}$ in (9), the latter condition of proper containment is seen to be equivalent to the condition that the corresponding points $\boldsymbol{\omega}$ and $\boldsymbol{\omega}'$ on $\mathrm{dS}^{(n+1)}$ are timelike or lightlike separated with $\boldsymbol{\omega}'$ to the future of $\boldsymbol{\omega}$ in the time orientation given by increasing t. This shows that the set-theoretic partial-order relation of spherical caps given by containment just corresponds to the partial-order relation on $\left(\mathrm{dS}^{(n+1)}, \boldsymbol{g}^{\mathrm{dS}^{(n+1)}}\right)$ given by causality. More precisely, $\boldsymbol{\omega}'$ lies to the causal future of $\boldsymbol{\omega}$ if the cap corresponding to $\boldsymbol{\omega}$ is properly contained in the cap corresponding to $\boldsymbol{\omega}'$. This causal separation is timelike if the smaller cap is properly contained in the interior of the larger one, and lightlike if the boundary spheres of the caps just touch at one point. (We will come back to this order relation in more detail when we discuss the images of caps of S^n under stereographic projection in $\mathbb{R}^n$, where they become balls.) It is intriguing that, in this way, Lie sphere geometry provides a natural link between causal- and cap- or 'sphere-orders'. In fact, this relation is inherent in the discussion of sphere orders in [8][4], the motivation of which came from causal orders, however without relating it to Lie sphere geometry.

2.2. Balls and oriented hyperspheres in flat Euclidean space

The foregoing construction also applies to balls, or oriented hyperspheres, in flat Euclidean space $\mathbb{R}^n$ if suitably generalised. To see this we regard S^n as one-point compactification of $\mathbb{R}^n$. The point added to $\mathbb{R}^n$ is called 'infinity' and denoted by ∞. The set $\mathbb{R}^n \cup \{\infty\}$ is topologised in such a way that complements of compact sets in $\mathbb{R}^n$ become open neighbourhoods of ∞, which makes $\mathbb{R}^n \cup \{\infty\}$ homeomorphic to S^n. A homeomorphism is given by inverse stereographic projection centred at, say, the 'south pole' $(0, \ldots, 0, -1)$; compare (B.2):

$$\mathbb{R}^n \ni \boldsymbol{x} \mapsto \boldsymbol{X} = \left(\frac{2\boldsymbol{x}}{1 + \boldsymbol{x}^2}, \frac{1 - \boldsymbol{x}^2}{1 + \boldsymbol{x}^2} \right) \in S^n \subset \mathbb{R}^{n+1}. \tag{12}$$

An important property of stereographic projections is that balls in $\mathbb{R}^n$ are mapped to spherical caps in S^n[5]. Consequently we can use Lie sphere geometry to also describe the configurations of balls, or oriented hyperspheres, in $\mathbb{R}^n$. As before, the n-sphere can be embedded into

---

[4] We thank Fay Dowker for pointing out this reference.

[5] Images of balls in $\mathbb{R}^n$ under (12) are spherical caps not containing ∞. Spherical caps containing ∞ in their interior or on their boundary are images under (12) of closures of complements of balls and images of half-spaces, respectively. This will be further discussed below.
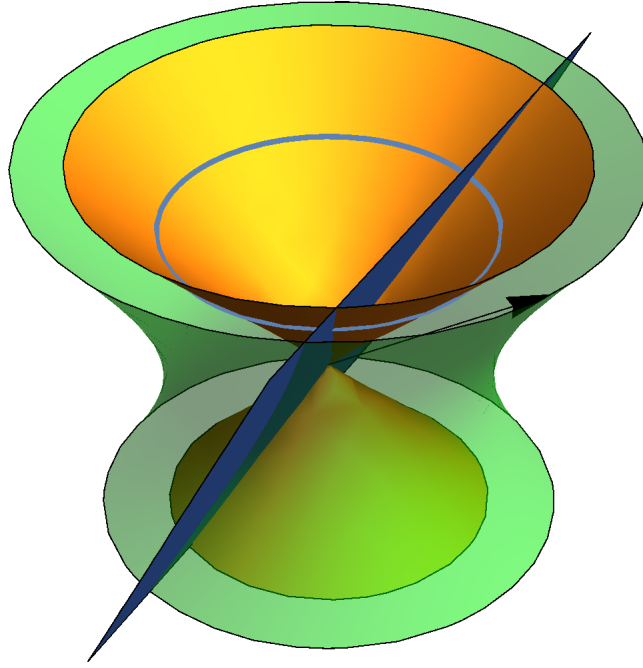
Figure 2. Illustration of the bijection between spherical caps or oriented hyperspheres in the Möbius sphere S^n and points on $dS^{(n+1)}$, here for $n = 1$. The picture shows various geometric objects embedded into $(1 + 2)$-dimensional Minkowski space: the 2-dimensional (2D) light-cone is depicted in yellow, the 2D hyperboloid of unit spacelike vectors, i.e. 2D deSitter space, in green. The Moebius sphere is the intersection of the light-cone with an affine hyperplane (not shown in the diagram) of constant unit time, here depicted by the light-blue circle. Finally, the oriented timelike hyperplane through the origin is in dark-blue and its (oriented) normal by the black arrow, denoted by ω in the text, whose tip defines a point on the green hyperboloid. This point uniquely defines a spherical cap of—or oriented hypersphere in—the Moebius sphere. Note that the closure of the complement of the spherical cap is also a spherical cap bounded by the same but oppositely oriented hypersphere, and both are represented by $-\omega$.

$\mathbb{R}^{(1,n+1)}$ (to become the Möbius sphere) via $\boldsymbol{\xi} = (1, \boldsymbol{X})$, where $\boldsymbol{X}$ is a unit vector in Euclidean $\mathbb{R}^{n+1}$, which is now to be expressed through $\boldsymbol{x}$ according to (12). A ball in $\mathbb{R}^n$ with centre $\boldsymbol{p}$ and radius $r > 0$ is defined as the set of all points $\boldsymbol{x}$ satisfying

$$(\boldsymbol{x} - \boldsymbol{p})^2 \leqslant r^2. \tag{13}$$

A short calculation shows that this is equivalent to

$$\langle \boldsymbol{\xi}, \boldsymbol{\omega} \rangle \geqslant 0, \tag{14}$$

where

$$\boldsymbol{\omega} = \left(\frac{1 + \boldsymbol{p}^2 - r^2}{2r}, \frac{\boldsymbol{p}}{r}, \frac{1 - \boldsymbol{p}^2 + r^2}{2r} \right) \in \mathbb{R}^{(1,n+1)} \tag{15}$$

is a spacelike unit vector in $(n + 2)$-dimensional Minkowski space $\mathbb{R}^{(1,n+1)}$.

Note that the closure of the complement of the ball described by (13) is described by the reversed inequality, $(x - p)^2 \geqslant r^2$, hence by $\langle \xi, \omega \rangle \leqslant 0$ instead of (14). Consequently, the complement of a ball represented by ω is represented by $-\omega$, just as before. We can use the same representation (15) if we associate a negative radius $r < 0$ to these sets. Hence, a Lie vector ω can represent either a ball (with positive and negative radius) using (15) or a spherical cap via (7).

However, not all points on de Sitter space can be parametrised by (15); we are missing those which are parametrised by

$$\omega = (-d, \boldsymbol{n}, d), \tag{16}$$

where $\boldsymbol{n}^2 = 1$. If we consider the scalar product $\langle \xi, \omega \rangle \geqslant 0$, we obtain

$$\boldsymbol{n} \cdot \boldsymbol{x} \geqslant d. \tag{17}$$

This is a half-space in $\mathbb{R}^n$ with a boundary plane with outward-pointing normal $\boldsymbol{n}$ and distance d from the origin. It can be shown that these half-spaces correspond to caps containing the south pole on their boundary. Hence, half-spaces can be interpreted as balls just touching infinity with their boundary. Altogether, there is a bijective correspondence between spherical caps on S^n on one side, and balls, their complements, and half-spaces in $\mathbb{R}^n$ on the other. We will use this fact to visualise caps on the 3-sphere as the corresponding objects in $\mathbb{R}^3$. The 2D case is shown in figure 3.

2.3. Intersecting caps, or oriented hyperspheres, and descartes configurations

From (15) we can easily calculate the Minkowskian inner product between two vectors ω_1 and ω_2 in $\mathbb{R}^{(1,n+1)}$ representing balls with parameters $(\boldsymbol{p}_1, r_1)$ and $(\boldsymbol{p}_2, r_2)$, respectively. The result is

$$\langle \omega_1, \omega_2 \rangle = \frac{r_1^2 + r_2^2 - \|\boldsymbol{p_1} - \boldsymbol{p_2}\|^2}{2r_1r_2} = \pm 1 + \frac{(r_1 \mp r_2)^2 - \|\boldsymbol{p_1} - \boldsymbol{p_2}\|^2}{2r_1r_2}. \tag{18}$$

Here the second equality holds either with both upper or both lower signs in the terms on the right-hand side. It immediately shows that $\langle \omega_1, \omega_2 \rangle \in [-1, 1]$ iff

$$|r_1 - r_2| \leqslant \|\boldsymbol{p}_1 - \boldsymbol{p}_2\| \leqslant |r_1 + r_2|, \tag{19}$$

with $\langle \omega_1, \omega_2 \rangle = -1$ for $\|\boldsymbol{p}_1 - \boldsymbol{p}_2\| = |r_1 + r_2|$ and $\langle \omega_1, \omega_2 \rangle = 1$ for $\|\boldsymbol{p}_1 - \boldsymbol{p}_2\| = |r_1 - r_2|$. It is geometrically clear that if $\|\boldsymbol{p}_1 - \boldsymbol{p}_2\| > |r_1 + r_2|$, i.e. if $\langle \omega_1, \omega_2 \rangle < -1$, the balls represented by ω_1 and ω_2 are disjoint; and that they just touch at a single boundary point, with oppositely pointing normals, if $\|\boldsymbol{p}_1 - \boldsymbol{p}_2\| = |r_1 + r_2|$, i.e. if $\langle \omega_1, \omega_2 \rangle = -1$. Moreover, if $\|\boldsymbol{p}_1 - \boldsymbol{p}_2\| < |r_1 - r_2|$, i.e. if $\langle \omega_1, \omega_2 \rangle > 1$, then either the ball represented by ω_1 is entirely contained in the interior of that represented by ω_2 (case $r_1 < r_2$) or vice versa (case $r_2 < r_1$). For $\|\boldsymbol{p}_1 - \boldsymbol{p}_2\| = |r_1 - r_2|$, i.e. $\langle \omega_1, \omega_2 \rangle = 1$, one ball is contained in the other with their boundaries touching at a single point with parallely pointing normals.

This shows that (19) is just the necessary and sufficient condition for the oriented boundary spheres of the balls to intersect. The angle between the normals at an intersection point is clearly independent of the intersection point and referred to as the *intersection angle* of the spheres. Applying the law of cosines to the triangle with vertices $\boldsymbol{p}_1$, $\boldsymbol{p}_2$, and an intersection point of the spheres with radii r_1 and r_2 centered at $\boldsymbol{p}_1$ and $\boldsymbol{p}_2$, respectively, immediately gives

$$\|\boldsymbol{p}_1 - \boldsymbol{p}_2\|^2 = r_1^2 + r_2^2 - 2r_1r_2 \cos(\gamma_{12}), \tag{20}$$
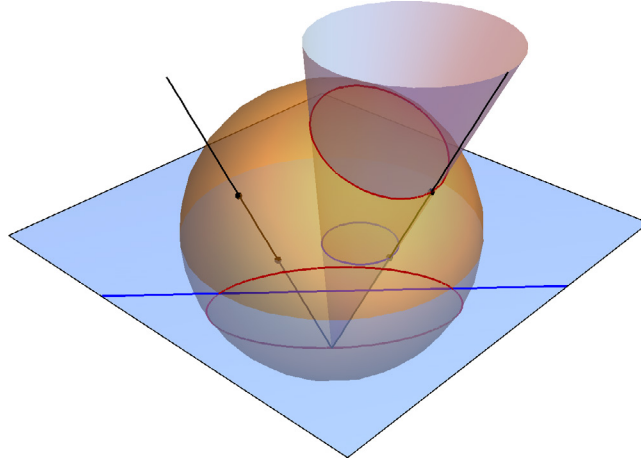
Figure 3. A Lie vector describes either a spherical cap or a ball/half-space.

where γ_{12} is the angle of the triangle at the intersection vertex, which is just the intersection angle of the spheres. Using (20) in the first equality of (18) leads to the simple formula

$$\langle \boldsymbol{\omega}_1, \boldsymbol{\omega}_2 \rangle = \cos(\gamma_{12}). \tag{21}$$

In particular, $\langle \boldsymbol{\omega}_1, \boldsymbol{\omega}_2 \rangle = 0$ means that the spheres intersect orthogonally, whereas $\langle \boldsymbol{\omega}_1, \boldsymbol{\omega}_2 \rangle = 1$ and $\langle \boldsymbol{\omega}_1, \boldsymbol{\omega}_2 \rangle = -1$ means that the spheres just touch tangentially with one containing the other in the first, and disjoint interiors in the second case.

On the n-sphere it is possible to find sets of (at most) $n + 2$ pairwise tangent caps. Such a set $\{\boldsymbol{\omega}_a : a = 1, \ldots, n + 2\}$ is called a *Descartes set*, in view of Descartes' circle theorem for four circles in flat two-dimensional space $\mathbb{R}^2$, giving a relation between the radii. The generalisation to higher dimensions was given by Soddy [39] and Gosset [27] in form of poems! There are several formulae which also include the centres and extensions to other constant-curvature spaces [35]. Lie sphere geometry provides an elegant and powerful unification of all these results.

Indeed, the caps of a Descartes set have to satisfy

$$\langle \boldsymbol{\omega}_a, \boldsymbol{\omega}_b \rangle = 2\delta_{ab} - 1 \tag{22}$$

because $\langle \boldsymbol{\omega}_a, \boldsymbol{\omega}_a \rangle = 1$ for all Lie vectors and $\langle \boldsymbol{\omega}_a, \boldsymbol{\omega}_b \rangle = -1$ if $a \neq b$ as condition for touching at one point. Writing the Descartes set as a square $(n + 2) \times (n + 2)$ matrix $\boldsymbol{W}$ whose rows are the components of the vectors $\boldsymbol{\omega}_a$, that is, $\boldsymbol{W}^\top = (\boldsymbol{\omega}_1, \ldots, \boldsymbol{\omega}_{n+2})$, we obtain the equivalent to (22):

$$\boldsymbol{W}\boldsymbol{\eta}\boldsymbol{W}^T = \boldsymbol{G}, \tag{23}$$

where $\boldsymbol{\eta} = \operatorname{diag}(-1, 1, \ldots, 1)$ is the Minkowski metric and $\boldsymbol{G}_{ab} = 2\delta_{ab} - 1$. Simply inverting (23) leads to (matrices with components $(2\delta_{ab} - 1)$ are non-singular in dimensions higher than two):

$$\boldsymbol{W}^T \boldsymbol{G}^{-1} \boldsymbol{W} = \boldsymbol{\eta}, \tag{24}$$

which is known as the *unified generalised Descartes theorem* containing formulae for centres as well as radii [35]. We shall be no more explicit at this point. But we think that the simple

half-page argument leading to (24), comprising the most general statement on the general Descartes' theorem, impressively demonstrates the ability of Lie sphere geometry.

Using the inverse of $\boldsymbol{G}$, we can define a set of *dual caps* (compare [40]) $\boldsymbol{\tau}_a$ via

$$\boldsymbol{\tau}_a := \kappa \sum_{b=1}^{n+2} (\boldsymbol{G}^{-1})_{ab} \, \boldsymbol{\omega}_b, \tag{25}$$

where $\kappa^2 = \frac{2n}{n-1}$ is needed for normalisation such that $\langle \boldsymbol{\tau}_a, \boldsymbol{\tau}_a \rangle = 1$. The components of the inverse matrix $\boldsymbol{G}^{-1}$ are given by $(\boldsymbol{G}^{-1})_{ab} = \frac{1}{2} \left(\delta_{ab} - \frac{1}{n} \right)$. The dual caps satisfy

$$\langle \boldsymbol{\tau}_a, \boldsymbol{\tau}_b \rangle = \frac{n \, \delta_{ab} - 1}{n - 1} \leqslant 1, \tag{26}$$

$$\langle \boldsymbol{\tau}_a, \boldsymbol{\omega}_b \rangle = \kappa \, \delta_{ab}, \tag{27}$$

showing that the cap $\boldsymbol{\tau}_a$ is orthogonal to all caps $\boldsymbol{\omega}_b$, $b \neq a$. Furthermore, the dual caps overlap in more than two dimensions, as the first equation shows.

2.4. Apollonian groups and the generation of Apollonian packings

The dual set just introduced can now be used to construct new spheres tangent to a given Descartes set. For this we define the mapping $\boldsymbol{I}_{\boldsymbol{\tau}_a}$ acting on the set of all Descartes sets via

$$\boldsymbol{\omega}_b' = \boldsymbol{I}_{\boldsymbol{\tau}_a} \boldsymbol{\omega}_b = \boldsymbol{\omega}_b - 2 \, \langle \boldsymbol{\omega}_b, \boldsymbol{\tau}_a \rangle \, \boldsymbol{\tau}_a. \tag{28}$$

In Minkowski space $\mathbb{R}^{(1,n+1)}$ it corresponds to a reflection in the timelike hyperplane with unit normal $\boldsymbol{\tau}_a$. Hence we have $\boldsymbol{\omega}_b' = \boldsymbol{I}_{\boldsymbol{\tau}_a} \boldsymbol{\omega}_b = \boldsymbol{\omega}_b$ if $b \neq a$, since $\langle \boldsymbol{\omega}_b, \boldsymbol{\tau}_a \rangle = 0$, since $\boldsymbol{\omega}_b$ lies in the hyperplane of reflection, which is clearly pointwise fixed. It can be easily verified that the set $\{ \boldsymbol{I}_{\boldsymbol{\tau}_a} \boldsymbol{\omega}_a, \boldsymbol{\omega}_b : b \neq a \}$ forms a new Descartes set. Being reflections, the maps $\boldsymbol{I}_{\boldsymbol{\tau}_a}$ clearly preserve the Minkowski inner product, i.e. they are Lorentz transformations, so that $\langle \boldsymbol{I}_{\boldsymbol{\tau}_a} \boldsymbol{\omega}_b, \boldsymbol{I}_{\boldsymbol{\tau}_a} \boldsymbol{\omega}_c \rangle = \langle \boldsymbol{\omega}_b, \boldsymbol{\omega}_c \rangle$. It can be shown that these maps also act on S^n and $\mathbb{R}^n$ by considering their points as spheres of radius zero. The hyperplane reflection $\boldsymbol{I}_{\boldsymbol{\tau}_a}$ then becomes an inversion on the sphere that is the boundary of the ball represented by $\boldsymbol{\tau}_a$. Let us recall that in $\mathbb{R}^n$ the map that inverts at a sphere with centre $\boldsymbol{p}$ and radius r is simply given by

$$\boldsymbol{x} \mapsto \boldsymbol{x}' := \boldsymbol{p} + \frac{r^2}{\|\boldsymbol{x} - \boldsymbol{p}\|^2} \, (\boldsymbol{x} - \boldsymbol{p}). \tag{29}$$

In passing we make the cautionary remark that whereas inversions map balls and spheres to balls and spheres, their centres will not be images of each other. For us a truly remarkable property will be important: namely that this correspondence of maps relates the non-linear inversion (29) to the *linear* hyperplane reflection (28). This will simplify calculations considerably and once more exemplifies the power of Lie sphere geometry, which gives a unified description for the flat and spherical case, which includes points and caps, as well as balls and half-spaces; see figure 4.

The mapping (28) $\{ \boldsymbol{\omega}_a \} \mapsto \{ \boldsymbol{\omega}_a' = \boldsymbol{I}_{\boldsymbol{\tau}_b} \boldsymbol{\omega}_a \}$ can also be written as follows

$$\boldsymbol{\omega}_a' = \sum_c (\boldsymbol{A}_b)_{ac} \, \boldsymbol{\omega}_c = \boldsymbol{\omega}_a, \qquad a \neq b, \tag{30}$$

$$\boldsymbol{\omega}_b' = \sum_c (\boldsymbol{A}_b)_{ac} \, \boldsymbol{\omega}_c = -\boldsymbol{\omega}_b + \frac{2}{n-1} \sum_{c \neq b} \boldsymbol{\omega}_c, \tag{31}$$
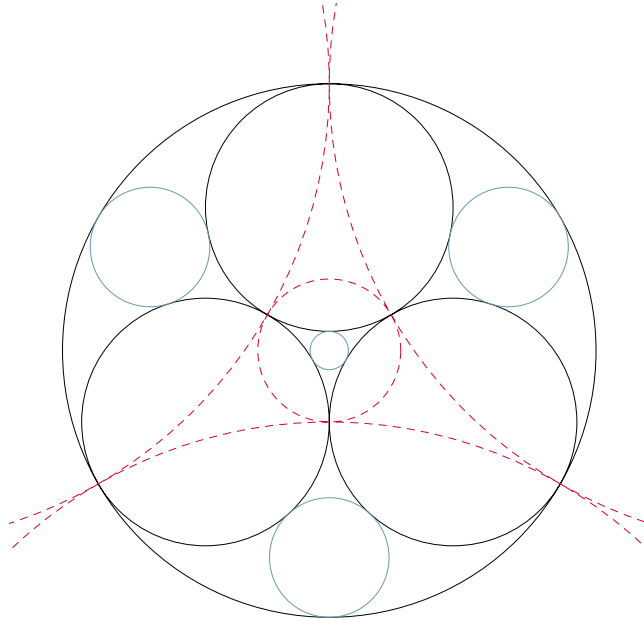
Figure 4. First iteration of a 2D Apollonian packing: initial set in black, dual set in red and reflected set in blue.

where A_b are the so-called *Apollonian matrices*. For example, in two and three dimensions, A_1 takes the form

$$A_1 = \begin{pmatrix} -1 & 2 & 2 & 2 \\ 0 & 1 & 0 & 0 \\ 0 & 0 & 1 & 0 \\ 0 & 0 & 0 & 1 \end{pmatrix}, \qquad A_1 = \begin{pmatrix} -1 & 1 & 1 & 1 & 1 \\ 0 & 1 & 0 & 0 & 0 \\ 0 & 0 & 1 & 0 & 0 \\ 0 & 0 & 0 & 1 & 0 \\ 0 & 0 & 0 & 0 & 1 \end{pmatrix}. \tag{32}$$

The group $\mathcal{A} = \langle A_1, \ldots, A_5 \rangle$ generated by the Apollonian matrices is called *Apollonian group* and was studied in [28–30]. It is a sub-group of the automorphism group of G^{-1}, that is, $A^t G^{-1} A = G^{-1}$, $A \in \mathcal{A}$. Equation (24) shows that the Apollonian group is conjugate to a sub-group of the Lorentz group. The inversions I act from the left on W^t, whereas elements A of the Apollonian group act from the left on W.

For $n = 2$ and $n = 3$, an orbit of the Apollonian group gives an 'almost-covering' of the n-sphere with non-overlapping spherical caps. This ceases to be true in higher dimensions because the Apollonian groups consists of integer matrices only in two and three dimensions. The residual sets of points not contained in any cap form fractals of Hausdorff dimension 1.3057 ($n = 2$) [28] and 2.4739 ($n = 3$) [7, 30]. Since the Lorentz group acts transitively on the set of all Descartes sets, one might say that there is only one Descartes set, and consequently only one Apollonian packing, up to Lorentz transformations.

The advantage in using the inversions I_{τ_b} rather than the Apollonian matrices A_b is that the former can act on single caps whereas the latter can only act on Descartes sets W. For this reason they are more useful for numerical calculations of Apollonian packings. Note that the

representation of the inversion matrices I_{τ_a} depends on the chosen Descartes set, whereas the Apollonian matrices are defined independently of any such choice.

In order to construct an Apollonian packing in two/three dimensions, we start with an initial Descartes set of four/five pairwise tangent caps on the 2-sphere/3-sphere. For this set we calculate the dual caps and determine the inversion matrices I. We can iteratively generate the Apollonian packing if we apply the inversions with respect to the initial dual set to all caps generated in the previous step, where the zeroth iteration is the initial set. This way we fill up the whole 2-sphere. However, in three dimensions, we generate several caps multiple times due to the overlapping of the dual caps. For our purposes and for numerical efficiency, we have to remove the duplicates. This we achieve by dividing the dual caps into target regions in such a way that each point is associated to only one target region. Therefore, we construct further caps whose boundaries cross the intersection points of the dual caps. New caps are accepted only if their centre lies within the target region of the inversion. This can easily be tested using the scalar product with the dividing caps. Remarkably, it is possible to calculate the exact positions and sizes of the caps without numerical errors since the coordinates take integer values. The stereographic projection of the Apollonian packing based on the regular pentatope (the four-dimensional analogue of the tetrahedron) is shown in figure 5.

In order to obtain more uniform packings without very big caps, as we, e.g. want to have for Friedmann-like configurations, it is possible to modify this procedure. To achieve this, we take the complement of a big cap and four new caps inside the former interior of the big cap, such that we obtain a new Descartes set. Now we repeat the procedure described above and generate another Apollonian packing in the former interior. In a final step, the complement of the original cap is removed. This is shown in figure 6. This procedure can be applied to all caps which are too big. Since all Apollonian packings are related by a Lorentz transformation, it is possible to construct a transformation which can be applied to the original packing and maps all caps except for one, which becomes the exterior, into the interior of a big cap.

3. Swiss-cheese models

We already mentioned in the introduction the so called swiss-cheese models for inhomogeneous cosmologies, the construction of which goes back to a seminal paper by Einstein and Straus [20]. Their construction is based on Friedmann dust universes in which spherical regions of dust are removed and replaced by exterior Schwarzschild geometries. Hence, the global behaviour of such a space-time is still given by the Friedmann equations but locally there are regions which are static and not influenced by the cosmic expansion. As we will use these models for comparison, we want to start by recalling how they are constructed. We use units in which $G = c = 1$, so that lenghts, times, and masses share the same unit. We will also restrict attention to spherical (positively curved) dust universes.

A spherical dust universe is described by the Friedmann–Lemaître–Robertson–Walker metric

$$\boldsymbol{g} = -\mathbf{d}t^2 + a^2(t)\left(\mathbf{d}\chi^2 + \sin^2\chi\,\mathbf{d}\Omega^2\right). \tag{33}$$

The spatial part is a round 3-sphere with a time-dependent radius $a(t)$, called scale factor. The latter is determined by the first Friedmann equation, here for $\Lambda = 0$,

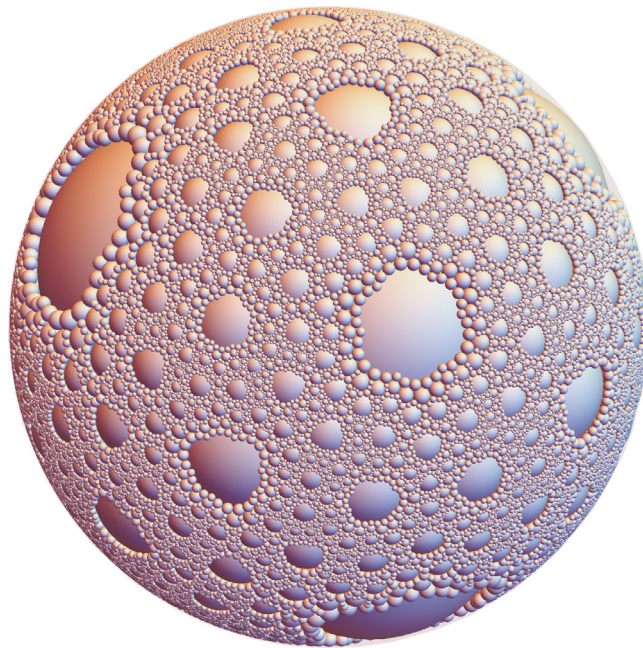$$\frac{\dot{a}^2}{a^2} = \frac{8\pi C}{3a^3} - \frac{1}{a^2}, \tag{34}$$

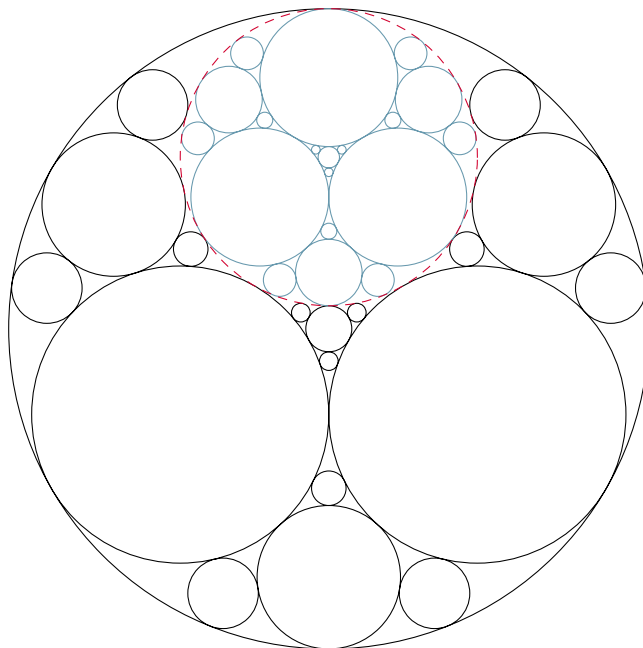**Figure 5.** Pentatope-based Apollonian packing with 1424 790 spheres.

Figure 6. Construction of more uniform packings: a big circle (red) is replaced by a smaller Apollonian packing.

where C is constant. Moreover, space is filled with spatially homogeneous dust, that is, an ideal fluid with vanishing pressure, $p \equiv 0$, and density given by

$$\rho(t) = \frac{C}{a^3(t)}. \tag{35}$$

Since the volume of the 3-sphere $V(t) = 2\pi^2 a^3(t)$ is finite, it is possible to define a total mass via $M = \rho(t)V(t) = 2\pi^2\rho(t)a^3(t) = 2\pi^2 C$ which is constant due to (35). The first Friedmann equation (34) can be solved and the well-known solution in parametric form is given by

$$a(\eta) = \frac{4\pi C}{3}(1 - \cos\eta), \tag{36}$$

$$t(\eta) = \frac{4\pi C}{3}(\eta - \sin\eta), \tag{37}$$

where $\eta \in (0, 2\pi)$. Hence, the scale factor follows a cycloid. The universe starts with a big bang and expands to a maximal size $a_0 = a(\eta = \pi) = \frac{8\pi C}{3}$. Then it recollapses and finally ends in a big crunch. It follows that the total mass is given by

$$M_{\text{tot}} = \frac{3\pi}{4}\, a_0. \tag{38}$$

We cut out the interior of a sphere centred at the north pole in the dust universe with areal radius $R = a(t)\chi_0$, where $\chi_0 = \text{const}$. Note that the amount of dust within that sphere is independent of t. We now replace the interior geometry, which had been of constant positive curvature, by that of an exterior Schwarzschild space-time describing a black-hole with mass m. The latter is given by

$$\boldsymbol{g} = -\left(1 - \frac{2m}{r}\right)\mathbf{d}T^2 + \left(1 - \frac{2m}{r}\right)^{-1}\mathbf{d}r^2 + r^2\,\mathbf{d}\Omega^2. \tag{39}$$

In these coordinates, the areal radius is just $R = r$. In order for this replacement to result in a regular solution to Einstein's equations, we have to satisfy the Israel junction conditions [31]. For spherically symmetric space-times, these conditions have been shown in [12] to be equivalent to the equality of some physically intuitive quantities on both sides of the matching spheres along which the two spac-times are glued together. According to [12] it is, in our case, sufficient to check the equality of together:

  (i) the areal radius R,
 (ii) the Misner–Sharp mass $\mathcal{M}$.

Note that the areal radius R is a function defined on any spherically symmetric space-time, the value of which at a given point p is defined to be $R(p) := \sqrt{A(p)/4\pi}$, where $A(p)$ is the 2D volume of the $SO(3)$ orbit containing p[6]. We note the following general expression of the Misner–Sharp mass in terms of the areal radius, the latter considered as a smooth function on space-time (assigning to each space-time point the 2D area of the $SO(3)$ orbit passing through it)

$$\mathcal{M} = \frac{R}{2}\left(1 - \boldsymbol{g}^{-1}\left(\mathbf{d}R, \mathbf{d}R\right)\right). \tag{40}$$

---

[6] We recall the definition of spherical symmetry: a space-time is called spherically symmetric if it allows for an effective $SO(3)$ action by isometries whose generic orbits are spacelike 2-spheres.

Equality of areal radii just means equality of the surface areas of the respective $SO(3)$ orbits that are to be identified. Equality of the Misner–Sharp masses then means that the norms of the differentials dR on these orbits to be pairwise identical same. Now, from (33) and (39) one immediately reads off that for the FLRW and Schwarzschild geometry the areal radii are respectively given by

$$R_{\text{FLRW}} = a(t) \sin \chi, \tag{41}$$

$$R_{\text{Schw}} = r. \tag{42}$$

Using this and the expression (40) for the Misner–Sharp mass, one immediately deduces that for FLRW and Schwarzschild the latter is respectively given by

$$\mathcal{M}_{\text{FLRW}} = \frac{1}{2}a(t)\big(\dot{a}^2(t) + 1\big) \sin^3 \chi = \frac{a_0}{2} \sin^3 \chi, \tag{43}$$

$$\mathcal{M}_{\text{Schw}} = m, \tag{44}$$

where in the second equality of the first equation for $\mathcal{M}_{\text{FLRW}}$ we have used (34) and that the constant C is related to the maximal scale factor a_0 through $a_0 = 8\pi C/3$, as already seen above.

Equality of (43) and (44) tells us that if a spherical cap of normalised geodesic radius χ (in units of $a(t)$) is removed from the FLRW universe and replaced by a Schwarzschild blackhole, the mass of the latter is given by

$$m = \frac{1}{2}a_0 \sin^3 \chi. \tag{45}$$

Equality of (41) and (42) then tells us that the areal radius of the vacuole without dust, in which the metric is just (39), is

$$r = a(t) \sin \chi. \tag{46}$$

It is time dependent because its boundary is clearly co-moving with the dust. The geometry inside this co-moving vacuole is strictly static

This procedure can be repeated for arbitrarily many black-holes, as long as as the Schwarzschild regions do not overlap. If we imagine the dust universe as cheese and the Schwarzschild regions as holes therein, the intuitive image of a 'swiss-cheese' becomes obvious. We can now construct general swiss-cheese models by generating Apollonian packings as described above. Every spherical cap of size χ is then turned into a Schwarzschild cell with a black-hole at the centre, whose (Misner–Sharp) mass equals that of the removed dust and which is hence determined by (45). Continuing in this fashion by filling in more and mode non overlapping spherical caps with static vacuum Schwarzschild geometries leaves us with as little dust matter as we please, and yet the time evolution outside the vacuoles is still exactly as in FLRW. We expect that a proper vacuum solution to Einstein's equations should be similar to a corresponding swiss-cheese model, which will serve us as a reference model.

4. Exact vacuum initial data

We wish to compare the swiss-cheese model with an exact vacuum solution with black-holes of the same masses at the same positions. And, as outlined in the introduction, the philosophy behind that is to eventually replace inhomogeneous matter distributions by inhomogeneous distributions of black-holes, in which case the time evolution is given by Einstein's *vacuum* equations. The hope connected with that procedure is to eventually achieve significant

simplifications in the analytical and numerical treatments, even though exact analytic time evolutions to the initial data representing many black-holes are not known. For the moment we are content with the fact that it is possible to analytically construct exact initial-data on a spacelike hypersurface of constant time representing general multi black-hole configurations.

In the $3 + 1$-formulation of general relativity, we consider time-evolving tensors on a three-dimensional (3D) manifold instead of tensors on space-time. This corresponds to a foliation of space-time by spacelike hypersurfaces and tensor fields restricted to these. The fundamental fields in this theory are the spatial metric $\boldsymbol{h}$ and the extrinsic curvature $\boldsymbol{K}$, both of which are symmetric, purely covariant (all indices down) second-rank tensors. For a general overview of this formalism and the classic references refer to [26], and to [3] for a comprehensive book and its use in numerical relativity.

In general relativity, initial data cannot be chosen freely but they have to satisfy the Hamiltonian and the momentum constraint, which in vacuum ($T_{\mu\nu} = 0$) and vanishing cosmological constant read

$$\mathcal{R}_{\boldsymbol{h}} + K^2 - K^a{}_b K^b{}_a = 0, \tag{47}$$

$$\nabla_b K^b{}_a - \nabla_a K = 0. \tag{48}$$

Here $\mathcal{R}_{\boldsymbol{h}}$ and ∇ are the Ricci scalar and Levi-Civita covariant derivative with respect to the spatial metric $\boldsymbol{h}$, respectively, and $K = h^{ab}K_{ab}$ is the trace of $\boldsymbol{K}$ with respect to $\boldsymbol{h}$. As initial hypersurface, we take a time-symmetric hypersurface characterised by the vanishing of the extrinsic curvature, $\boldsymbol{K} \equiv 0$. This corresponds to a state in which the black-holes are momentarily at rest. Such a solution should correspond to a dust universe at the moment of maximal expansion, when the scale factor becomes a_0. For time-symmetric initial data, the momentum constraint (48) is satisfied identically and the Hamiltonian constraint (47) reduces to the condition of scalar-flatness for the metric $\boldsymbol{h}$. To satisfy the latter, we make the conformal ansatz

$$\boldsymbol{h} = \Psi^4 \tilde{\boldsymbol{h}} \tag{49}$$

and read the condition for scalar-flatness as condition for Ψ, whereas the conformal metric $\tilde{\boldsymbol{h}}$ remains freely specifiable. As will be discussed in more detail below (compare (56)), this leads to an elliptic differential equation for Ψ, usually referred to as *Lichnerowicz equation*, which in our case reads:

$$\tilde{\Delta}\Psi - \frac{1}{8}\tilde{\mathcal{R}}\,\Psi = 0. \tag{50}$$

Here $\tilde{\Delta} = \tilde{h}^{ab}\tilde{\nabla}_a\tilde{\nabla}_b$ is the Laplacian with respect to the conformal metric $\tilde{\boldsymbol{h}}$. In view of the cosmological solution (33), the conformal metric is chosen to be that of a round unit 3-sphere[7]

$$\tilde{\boldsymbol{h}} = \boldsymbol{h}_{S^3} = \mathbf{d}\chi^2 + \sin^2\chi\,\mathbf{d}\Omega^2, \tag{51}$$

where (χ, θ, φ) are 3D polar angles and $\mathbf{d}\Omega^2 := \mathbf{d}\theta^2 + \sin^2(\theta)\,\mathbf{d}\varphi^2$ is the metric of the round unit 2-sphere S_1^2. The Ricci scalar of (51) is given by $\tilde{\mathcal{R}} = 6$ so that the Lichnerowicz equation (50) simply becomes

$$\tilde{\Delta}\Psi - \frac{3}{4}\Psi = 0. \tag{52}$$

Remarkably, this differential equation is linear so that the set of solutions is a linear space and the superposition principle applies. Note also that solutions cannot be globally regular on S^3

---

[7] Here and in the sequel S^3 always refers to the *unit* 3-sphere.

and must diverge somewhere. (Proof: multiply (52) with Ψ and integrate over S^3. Assuming regularity, the integral on the left is shown to be strictly negative after integration by parts without boundary terms, unless $\Psi \equiv 0$; a contradiction!) The non-regular points will be removed without introducing any (geodesic- and Cauchy-) incompleteness in the manifold $S^3 - \{\text{non regular points}\}$ with Riemannian metric $\boldsymbol{h}$. This is because the diverging Ψ will send the non-regular points to an infinite distance with respect to the metric $\boldsymbol{h} = \Psi^4 \tilde{\boldsymbol{h}}$. After point excision, the remaining neighbourhood of each point is an asymptotically flat end of the initial-data 3-maifold and represents a black hole.

4.1. Time symmetric multi black-hole solutions to Lichnerowicz equation

Linearity allows to give solutions to (52) for an arbitrary number of black-holes. They are easily written down if we think of the unit S^3 embedded in Euclidean $\mathbb{R}^4$. If we write $\boldsymbol{X}$ for the point of the 3-sphere (which one may think of as being parametrised by, say, the polar angles $(\chi, \vartheta, \varphi)$ or, alternatively, Euler angles $(\psi, \vartheta, \varphi)$, if one prefers to think in terms of coordinates, though we will not make use of such coordinatisations) and $\| \cdot \|$ for the standard (Euclidean) norm of $\mathbb{R}^4$, the solution for a number N of black-holes is then given by

$$\Psi(\boldsymbol{X}) = \sum_{i=1}^{N} \frac{\mu_i}{\|\boldsymbol{X} - \boldsymbol{P}_i\|}. \tag{53}$$

The solution property for each of the N terms is proven in detail in (A.1), as a special case of a more general theorem that works in all dimensions. Figure 7 provides an illustration of the graph for the function (53).

The point $\boldsymbol{P}_i \in S^3$ corresponds to the 'position' of the ith black-hole and the parameters μ_i are related to the masses by the expressions

$$m_i = 2 \sum_{\substack{j=1 \\ j \neq i}}^{N} \frac{\mu_j \mu_i}{\|\boldsymbol{P}_j - \boldsymbol{P}_i\|} \qquad (1 \leqslant i \leqslant N), \tag{54}$$

which we will derive below. The N points $\boldsymbol{P}_i$ where the solution diverges are removed from the manifold without introducing any incompletenesses. In fact, for $\boldsymbol{X} \to \boldsymbol{P}_i$ the metric is asymptotically flat and we will refer to this region as an 'end'[8]. Topologically the manifold is the N-fold punctured S^3. This solution is also discussed in [17] and [5] in slightly different but equivalent presentations. Our presentation (53) makes use of the simple embedding geometry of $\mathbb{R}^4$, which leads to simpler expressions and is much better adapted to later applications of Lie sphere geometry. But for completeness and comparison we note that the $\mathbb{R}^4$-distance $\|\boldsymbol{X} - \boldsymbol{Y}\|$ and the intrinsic geodesic distance (compare (2)) $\Lambda = \Lambda(\boldsymbol{X}, \boldsymbol{Y}) := \arccos(\boldsymbol{X} \cdot \boldsymbol{Y})$ between two points $\boldsymbol{X}$ and $\boldsymbol{Y}$ on S^3 are simply related by $\|\boldsymbol{X} - \boldsymbol{Y}\| = \sqrt{2(1 - \cos(\Lambda))} = 2 \sin(\Lambda/2)$. This is the way the solution was recently presented and discussed in [5, 18], with generalisation to non-vanishing cosmological constant in [19].

4.2. Isometry to Brill–Lindquist data

It is instructive to note that the solution just found is just the same (i.e. isometric to) as the good old Brill–Lindquist initial data sets [9] for $(N - 1)$ black-holes in an asymptotically flat 3-manifold the topology of which is that of a $(N - 1)$-fold punctured $\mathbb{R}^3$. In fact, there are N

---

[8] The notion of 'end' for a topological space was introduced by Freudenthal [23]. Roughly speaking, an end is a connected component in the complement of arbitrarily large compact sets.
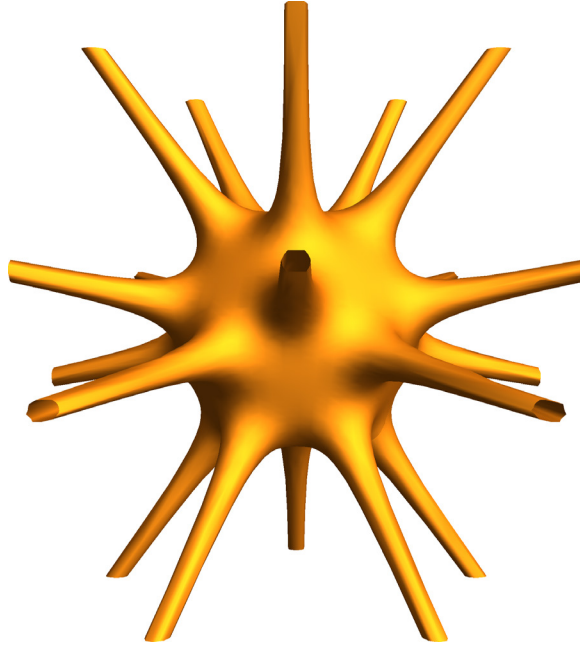
Figure 7. Plot of the function Ψ given in (53) over the 3-sphere, here represented as 2-sphere. It diverges at the N poles $\boldsymbol{P}_i$ which are deleted from the manifold. Neighbourhoods of the deleted points where Ψ is large then correspond to asymptotically flat ends, of which there are N, and which are geodesically complete.

isometries of our solution to such Brill–Lindquist sets, given by the stereographic projections $\pi : S^3 - \{\boldsymbol{P}\} \to \mathbb{R}^3$, where the pole $\boldsymbol{P}$ of the projection is chosen to be any of our black-hole positions $\boldsymbol{P}_i$, followed by a constant rescaling $\boldsymbol{x} \mapsto \boldsymbol{x}' := (\mu_i^2/2)\,\boldsymbol{x}$.

Before writing out the details of this isometry, let us point out that its existence is obvious from the conformal properties of the Laplacian and the conformal flatness of the metric $\boldsymbol{h}_{S^3}$ of the unit 3-sphere, expressed in formula (B.9) of appendix B. Quite generally, the following is true (see, e.g. [26] for proofs and further details): let $(M, \boldsymbol{g})$ be a (Semi-) Riemannian manifold of dimension $n > 2$ and consider on $C^\infty(M, \mathbb{R})$ the $\boldsymbol{g}$-dependent linear differential operator (sometimes called the 'conformal Laplacian')

$$\mathcal{D}_{\boldsymbol{g}} := \Delta_{\boldsymbol{g}} - \frac{n-2}{4(n-1)}\mathcal{R}_{\boldsymbol{g}}, \tag{55}$$

where $\Delta_{\boldsymbol{g}}$ and $\mathcal{R}_{\boldsymbol{g}}$ denote the Laplacian and Ricci scalar with respect to $\boldsymbol{g}$, respectively. Let M_Ω denote the linear operator in $C^\infty(M, \mathbb{R})$ that multiplies each element with $\Omega \in C^\infty(M, \mathbb{R}_+)$. Then the following relation holds:

$$\mathcal{D}_{\Omega^{\frac{4}{n-2}}\boldsymbol{g}} = M_{\Omega^{-\frac{n+2}{n-2}}} \circ \mathcal{D}_{\boldsymbol{g}} \circ M_\Omega. \tag{56}$$

In $n = 3$ dimensions we have $\mathcal{D}_{\boldsymbol{g}} = \Delta_g - (1/8)\mathcal{R}_g$. Equation (56) and conformal flatness[9] of the unit-sphere metric, i.e. $\boldsymbol{h}_{S^3} = \Omega^4 \boldsymbol{h}_{\mathbb{R}^3}$, immediately imply that if Ψ is in the kernel of $\mathcal{D}_{\boldsymbol{h}_{S^3}}$, i.e. solves (52), then $\Omega \cdot \Psi$ is in the kernel of $\mathcal{D}_{\boldsymbol{h}_{\mathbb{R}^n}} = \Delta_{\boldsymbol{h}_{\mathbb{R}^n}}$ and hence harmonic. The latter are

---

[9] Here and in the sequel $\mathbb{R}^3$ denotes flat Euclidean 3-space endowed with with its natural coordinates x^a in which the flat metric is $\boldsymbol{h}_{\mathbb{R}^3} = \sum_{a=1}^3 \mathbf{d}x^a \otimes \mathbf{d}x^a = \mathbf{d}\boldsymbol{x} \bar{\otimes} \mathbf{d}\boldsymbol{x}$.

the solutions to the Lichnerowicz equation in the conformally flat Brill–Lindquist case, the former are our solutions in the conformally spherical cosmological case. Hence we see that they are just related by multiplication with (a constant multiple of) Ω. This we will now show more explicitly.

We are interested in the explicit form of this isomorphism, for that will provide analytic expressions relating the parameters μ_i with the familiar expressions for the ADM-masses of the black-holes. For the reader's convenience we have collected the relevant facts and formulae concerning stereographic projections and its metric properties in appendix B in an essentially coordinate independent form. Given these formulae, the explicit proof of isometric equivalence is easy. We write (49) with $\tilde{\boldsymbol{h}} = \boldsymbol{h}_{S^3}$, replace $\boldsymbol{h}_{S^3}$ according to (B.9) with the flat metric $\boldsymbol{h}_{\mathbb{R}^3}$ and replace Ψ with the right-hand side of (53); this gives:

$$\boldsymbol{h} = \left(\sum_{i=1}^{N} \frac{\mu_i}{\|\boldsymbol{X} - \boldsymbol{P}_i\|} \right)^4 \frac{\|\boldsymbol{X} - \boldsymbol{P}\|^4}{4} \, \boldsymbol{h}_{\mathbb{R}^3}. \tag{57}$$

Now we choose any of the black-hole 'positions' $\boldsymbol{P}_i$ as center $\boldsymbol{P}$ for the stereographic projection, say $\boldsymbol{P} = \boldsymbol{P}_N$. Then

$$\boldsymbol{h} = \left(1 + \sum_{i=1}^{N-1} \frac{\mu_i}{\mu_N} \frac{\|\boldsymbol{X} - \boldsymbol{P}_N\|}{\|\boldsymbol{X} - \boldsymbol{P}_i\|} \right)^4 \frac{\mu_N^4}{4} \, \mathbf{d}\boldsymbol{x} \dot{\otimes} \mathbf{d}\boldsymbol{x}. \tag{58}$$

Setting $\boldsymbol{P} = \boldsymbol{P}_N$ and $\boldsymbol{Y} = \boldsymbol{P}_i$ in equation (B.6) of appendix B shows that

$$\frac{\|\boldsymbol{X} - \boldsymbol{P}_N\|}{\|\boldsymbol{X} - \boldsymbol{P}_i\|} = \frac{2}{\|\boldsymbol{P}_i - \boldsymbol{P}_N\|} \cdot \frac{1}{\|\boldsymbol{x} - \boldsymbol{p}_i\|}, \tag{59}$$

where $\boldsymbol{x}$ and $\boldsymbol{p}_i$ are the images of $\boldsymbol{X}$ and $\boldsymbol{P}_i$ under the stereographic projection. Hence (58) can be rewritten into

$$\boldsymbol{h} = \left(1 + \sum_{i=1}^{N-1} \frac{\lambda_i}{\|\boldsymbol{x}' - \boldsymbol{p}_i'\|} \right)^4 \mathbf{d}\boldsymbol{x}' \dot{\otimes} \mathbf{d}\boldsymbol{x}', \tag{60}$$

where $\boldsymbol{x}' := (\mu_N^2/2)\, \boldsymbol{x}$, $\boldsymbol{p}_i' := (\mu_N^2/2)\, \boldsymbol{p}_i$, and

$$\lambda_i := \frac{\mu_i \mu_N}{\|\boldsymbol{P}_i - \boldsymbol{P}_N\|}. \tag{61}$$

Equation (61) are precisely the Brill–Lindquist data for $(N-1)$ black-holes at positions $\boldsymbol{p}_i' = (\mu_N/2)\, \pi(\boldsymbol{P}_i)$. The manifold is $\Sigma := \mathbb{R}^3 - \{\boldsymbol{p}_1', \cdots, \boldsymbol{p}_{N-1}'\}$ with coordinates $\boldsymbol{x}'$ with respect to which the initial metric is the canonical flat metric $\mathbf{d}\boldsymbol{x}' \cdot \mathbf{d}\boldsymbol{x}'$. The Riemannian manifold $(\Sigma, \boldsymbol{h})$ is complete with N asymptotically flat ends, one for $\|\boldsymbol{x}'\| \to \infty$ (spacelike infinity) and $(N-1)$ 'internal' ones, one for each $\boldsymbol{x}' \to \boldsymbol{p}_i'$, where $i = 1, \cdots, (N-1)$.

4.3. ADM masses

Quite generally, an ADM mass can be associated to any asymptotically flat end of a 3-manifold in a purely geometric fashion [1]; for applications compare also [26]). The invariant geometric character of this association allows to compute the ADM mass in suitable coordinates. A convenient way to do this is to asymptotically put the metric towards the flat end into the form of the spatial part of the exterior Schwarzschild metric in so-called isotropic coordinated (which also manifestly display conformal flatness). Then the metric takes the form

$$h_{\text{Schw}} = \left(1 + \frac{m}{2r}\right)^4 (\mathbf{d}r \otimes \mathbf{d}r + r^2 \, h_{S^2}), \tag{62}$$

where m is the ADM-mass in geometric units (i.e. $m = GM/c^2$, where M is the mass in SI-units) and h_{S^2} denotes the standard round metric on the unit 2-sphere.

In our case, there is one such ADM mass for each of the N ends of (Σ, h). That at spatial infinity we call m_N, for on S^3 it corresponds to the black-hole at $\boldsymbol{P}_N$. Here, in the Brill–Lindquist picture, it corresponds to the total mass/energy of space-time, that is composed of all the contributions of all $(N-1)$ black-holes, diminished by the (negative) binding energy (compare the discussions in [9] and [26]). Direct comparison of (60) for $\|\boldsymbol{x}'\| \to \infty$ with (62) immediately gives

$$m_N = 2 \sum_{i=1}^{N-1} \lambda_i = 2 \sum_{i=1}^{N-1} \frac{\mu_i \mu_N}{\|\boldsymbol{P}_i - \boldsymbol{P}_N\|}. \tag{63}$$

The other masses can also be directly computed within the same stereographic projection, as we will show next. However, we can, in fact, immediately tell the result without any further calculation. This is true because we could have chosen any of the points $\boldsymbol{P}_j$ as centre for the stereographic projection, which would have resulted in the corresponding formula to (63), with j, rather than N, being the distinguished index. This indeed just leads to (54).

Despite this latter argument is elegant and certainly correct, we still wish to show how one arrives at the same result within the same stereographic projection centred at $\boldsymbol{P}_N$. The reason is that this calculation is instructive insofar as it shows how a well known expression for black-hole masses in the conformally flat Brill–Lindquist approach are rendered much more symmetric in the conformally spherical cosmological approach discussed here. The direct calculation proceeds as follows: for any $1 \leqslant i \leqslant (N-1)$ choose 'inverted' spherical polar coordinates $(\rho_i, \theta, \varphi)$ based at $\boldsymbol{p}'_i$, where $\rho_i := \lambda_i^2 / \|\boldsymbol{x}' - \boldsymbol{p}'_i\|$. The limit $\boldsymbol{x}' \to \boldsymbol{p}_i$ then corresponds to $\rho_i \to \infty$. In these coordinates the metric then assumes the form (62) with $r = \rho_i$ and

$$m = m_i := 2\lambda_i \left(1 + \sum_{j \neq i} \lambda_j / \|\boldsymbol{p}'_j - \boldsymbol{p}'_i\|\right) \qquad (1 \leqslant i \leqslant (N-1)). \tag{64}$$

This formula for the mass of a single hole in the metric (60) is well known from [9]. Now, replacing all λ_i according to (61), setting $\|\boldsymbol{p}'_j - \boldsymbol{p}'_i\| = \mu_N^2 / 2\|\boldsymbol{p}_j - \boldsymbol{p}_i\|$ and replacing $\|\boldsymbol{p}_j - \boldsymbol{p}_i\|$ by means of (B.6) with $\boldsymbol{x} = \boldsymbol{p}_i$, $\boldsymbol{y} = \boldsymbol{p}_j$, and $\boldsymbol{P} = \boldsymbol{P}_N$ then gives indeed (54). Note that the $(N-1)$ expressions (64) for the individual holes all look the same, but clearly different from the expression given by the first equality in (63) for the overall energy of all $(N-1)$ holes taken together, whereas in the conformally spherical cosmological picture the $(N-1) + 1 = N$ expressions (54) are again symmetric.

4.4. Geometry and topology

Finally we wish to mention a few more aspects in connection with the geometry and topology of the initial-data surface $\Sigma := \mathbb{R}^3 - \{\boldsymbol{p}'_1, \cdots, \boldsymbol{p}'_{N-1}\}$ in the Brill–Lindquist picture. Its geometry is conformally flat, $h = \Psi^4 h_{\mathbb{R}^3}$, where Ψ satisfies Laplace's equation $\Delta_{\mathbb{R}^3} \Psi = 0$, which is what Lichnerowicz's equation reduces to in this case. The solution given in (60), i.e.

$$\Psi(\boldsymbol{x}') = 1 + \sum_{i=1}^{N-1} \frac{\lambda_i}{\|\boldsymbol{x}' - \boldsymbol{p}'_i\|}, \tag{65}$$

is essentially a sum of $(N - 1)$ monopoles without contributions from higher multipoles. One might wonder why higher multipoles were excluded. The answer is that any such higher multipole would render the metric $\boldsymbol{h}$ incomplete (Ψ acquires zeros). Without higher multipoles, each monopole renders the manifold asymptotically flat in a neighbourhood of its location $\boldsymbol{p}_i'$ and introduces one end to which an ADM mass can be associated. Also associated to each end is an outermost (as seen from the end) minimal surface which, since we consider time-symmetric initial data, is an apparent horizon. In that sense the initial data set contains $(N - 1)$ black-holes. Note also that Σ is connected and simply connected, but with non-trivial second homology group given by

$$H_2(\Sigma, \mathbb{Z}) = \mathbb{Z}^{N-1}, \tag{66}$$

which in this case (i.e. due to simple connectedness) is also isomorphic to the second homotopy group $\pi_2(\Sigma)$. Each of the $(N - 1)$ factors $\mathbb{Z}$ in (66) is generated by one of the apparent horizons. There may be additional minimal surfaces corresponding to other elements of (66), like the sums of generators, which enclose the corresponding set of black-holes if their positions are chosen sufficiently close together (the individual holes may then be said to have merges into a composite black-hole). In the extreme case, where *all* the $(N - 1)$ holes are sufficiently close, there will be an Nth minimal surfaces enclosing all of them and corresponding to the sum all all generators in (66). This is the situation we have in mind if we speak of N black-holes on the 3-sphere. But note that in our original conformally spherical picture, adding just a single pole results in flat space without any black-hole and adding two poles merely results in the outer Schwarzschild geometry representing a single hole. For $N > 2$ poles the data result in at least $N - 1$ black-holes, and possibly N if the data are suitably chosen.

Finally we remark that the solution corresponding to the swiss-cheese model is obtained if we take the centres of the spherical caps for $\boldsymbol{P}_i$ and the mass parameters are obtained by solving the coupled system (54) of quadratically equations for μ_i, which can be done only numerically.

5. Unifoamy configurations

We have two solutions with Schwarzschild(-like) black-holes of the same masses at the same positions: the swiss-cheese model at the moment of maximal expansion and the initial data. Which Friedmann dust universe approximates such a solution best? In the former case, we simply take the dust universe of the model. In the latter case, we expect a similar value if most of the dust in the corresponding swiss-cheese model is removed. Clearly, not every configuration of black-holes resembles a Friedmann dust universe. Therefore, the black-holes should be distributed somehow evenly on the 3-sphere. However, there is no general notion on a uniform distribution of points on the 3-sphere and the definition of uniformity depends on the problem. Our approach is as follows: the mean inverse distance between two points in a uniform density distribution, $\rho = \text{const}$, is given by

$$\left\langle \frac{1}{\|\boldsymbol{P}_i - \boldsymbol{P}_j\|} \right\rangle = \frac{1}{2\pi^2} \int_0^\pi \mathrm{d}\chi \int_0^\pi \mathrm{d}\vartheta \int_0^{2\pi} \mathrm{d}\varphi \, \sin^2\chi \sin\vartheta \, \frac{1}{\sqrt{2(1 - \cos\chi)}} = \frac{8}{3\pi}, \tag{67}$$

using a coordinate system such that one point is located at the north pole. For a discrete configuration of equal black-holes, we simply demand the discrete analogue, namely

$$\left\langle \frac{1}{\|\boldsymbol{P}_i - \boldsymbol{P}_j\|} \right\rangle = \frac{1}{N} \sum_{j \neq i} \frac{1}{\|\boldsymbol{P}_i - \boldsymbol{P}_j\|} = \frac{8}{3\pi} \tag{68}$$

for all points $\boldsymbol{P}_i$. In the general case, we weight the inverse distances with the mass parameters, yielding

$$\left\langle \frac{1}{\|\boldsymbol{P}_i - \boldsymbol{P}_j\|} \right\rangle = \frac{1}{\sum_{k \neq i} \mu_k} \sum_{j \neq i} \frac{\mu_j}{\|\boldsymbol{P}_i - \boldsymbol{P}_j\|} = \frac{8}{3\pi}. \tag{69}$$

If we multiply this equation with $2\mu_i$, we obtain after a rearrangement

$$m_i = \sum_{j \neq i} \frac{2\mu_i \mu_j}{\|\boldsymbol{P}_i - \boldsymbol{P}_j\|} = \frac{16}{3\pi} \sum_{j \neq i} \mu_i \mu_j. \tag{70}$$

Hence, our condition for Friedmann-like configurations constrains the mass of each black-hole which is now essentially determined by its mass parameter irrespectively of the positions of all other black-holes on the 3-sphere in this case. This condition also guarantees that the black-holes are not too close to each other. We call configurations satisfying (70) *unifoamy* since it seems that the corresponding swiss-cheese model consists of evenly distributed Schwarzschild cells or, illustratively, a *uniform foam* of Schwarzschild bubbles. This is illustrated in figure 8. In passing we note that unifoamy configurations can be related to *central configurations*; compare [2] for the general notion and [21] for applications to Newtonian cosmology. Central configurations come into play if, for a fixed set of parameters μ_i, we ask for the set of positions $\boldsymbol{P}_i$ on S^3 for which the sum of masses m_i according to (70), i.e. the function $\sum_i \sum_{j \neq i} 2\mu_i \mu_j / \|\boldsymbol{P}_i - \boldsymbol{P}_j\|$, takes its minimal value. Adding the N constraints $\boldsymbol{P}_i^2 - 1 = 0$ with N Lagrange multipliers λ_i and carrying out the variation with respect to each position $\boldsymbol{P}_i$ and each multiplier λ_i results in equations which for $\lambda_i = C\mu_i$ turn into the equations for central configurations [22].

In order to be similar to a spherical Friedmann dust universe, we have to fit two parameters: the size a_0 and the total mass M. We set the total mass of the black-holes to $M = \sum_i m_i$. Since the size and the total mass of a spherical dust universe are related by (38), it appears to be natural to take this as the definition of the fitted size. Hence, we obtain for the size

$$A_0 = \frac{4}{3\pi} M = \frac{4}{3\pi} \sum_i m_i = \frac{64}{9\pi^2} \sum_i \sum_{j \neq i} \mu_i \mu_j. \tag{71}$$

For this reason, the total mass automatically fits to the dust universe and we only have to argue that our choice A_0 for the size also fits. This means that, comparing the spatial metric of a dust universe with the one of the black-hole initial data, the deviation of Ψ^2 from the fitted size A_0 should be small in the far-field region of the black-holes. Clearly, the deviation is large in the vicinity of the black-holes. We are not expecting that the space resembles a dust universe close to a black-hole in correspondence with our Universe in which local dynamics in the regime of galaxies strongly differ from the behaviour of the Universe on cosmic scales.

For a large number of black-holes, our result is approximately the same as that obtained by Korzyński by an ad-hoc averaging procedure [32]. He averaged the conformal factor Ψ over the 3-sphere with respect to the round metric, yielding

$$\langle \Psi \rangle = \frac{1}{2\pi^2} \int_{S^3} \Psi \, dV = \frac{64}{9\pi^2} \sum_{i,j} \mu_i \mu_j \approx A_0. \tag{72}$$
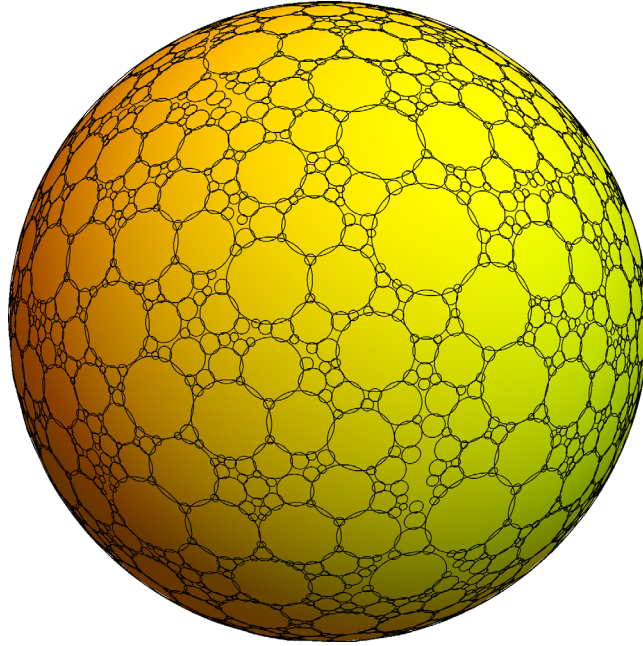
Figure 8. Two-dimensional illustration of the Lindquist-Wheeler model of a unifoamy configuration (the central black-holes are not plotted). The cells are distributed quite evenly on the sphere, they are not too big and do not overlap too much. Since this pictures gives the impression of a uniform foam on a sphere, we called such configurations 'unifoamy'.

Korzyński could give upper bounds for the deviation of the conformal factor from its average. The main parameters are the distance to the closest black-hole with respect to the round metric and the so-called modified spherical cap discrepancy $\mathcal{E}$ which is a quite abstract object and difficult to compute for a particular configuration. However, for particular configurations it is possible to estimate the cap discrepancy as follows. If we divide the 3-sphere in non-overlapping regions $\mathcal{V}_i$ such that the whole 3-sphere is covered and each region contains a black-hole whose mass parameter is proportional to the volume of the region, $\mu_i = \kappa \operatorname{vol} \mathcal{V}_i$, the spherical cap discrepancy is bounded from above by the largest diameter of all regions, that is,

$$\mathcal{E} \leqslant \max_{i=1,\dots,N} \operatorname{diam} \mathcal{V}_i, \tag{73}$$

where $\operatorname{diam} \mathcal{V}_i = \sup_{\boldsymbol{X},\boldsymbol{Y} \in \mathcal{V}_i} \Lambda(\boldsymbol{X}, \boldsymbol{Y})$. If we consider a configuration which is generated by an Apollonian packing, it should be possible to slightly deform the spherical caps such that the estimate is still approximately valid and given by the largest size χ_0 of all spherical caps,

$$\mathcal{E} \lesssim 2\chi_0. \tag{74}$$

The mass of the black-holes is related to the size of the spherical cap by (45). If we substitute the size a_0 by the total mass according to (38), now simply writing M instead of M_{tot}, and solve for the size χ, we obtain

$$\chi = \arcsin\left[\left(\frac{3\pi}{2M} m_i\right)^{1/3}\right]. \tag{75}$$

Hence, a good estimate for the spherical cap discrepancy should be given by

$$\mathcal{E} \lesssim 2\kappa \arcsin \left[\left(\frac{3\pi}{2M} \max m_i \right)^{1/3} \right]. \tag{76}$$

Therefore, we expect for configurations of black-holes with similar masses, that the deviation of the conformal factor from its average decreases in most regions because the cap discrepancy decreases with an increasing number of black-holes in this case. Since $\langle \Psi \rangle^2 \approx A_0$, the same should hold for our fit A_0. Hence, the space is almost round as it should be for a spherical dust universe. In particular, the minimum of the conformal factor $\Psi_{\min}$, which is taken in the far field of the black-holes, should be close to averaged value and therefore $\Psi_{\min}^2 \approx A_0$.

6. Comparison and discussion

Finally, we want to compare the different fits for the size to initial data configurations with the corresponding reference model. By this we mean the swiss-cheese model with black-holes located at the same positions and endowed with the same masses. For a good approximation, we expect that the fitted size is close to the size of the reference model, that is, the radius a_0 of the dust universe in the swiss-cheese model.

We consider the configurations with black-holes on the centres $\boldsymbol{P}_i$ of the spheres in the Apollonian packings as presented above. The masses m_i of the black-holes are given by the opening angles α_i of the spherical caps via (45). The mass parameters μ_i for the initial data can only be obtained numerically by solving the system of quadratic equation (54). This takes by far most of the computational effort, so that we have to limit the number of black-holes to about 10^5.

First, we consider the configurations obtained from the pentatope-based Apollonian packings shown in figure 5. We calculate the different possibilities for the fitted radius:

  (i) our suggestion A_0 from (71) for unifoamy configurations,
 (ii) Korzyński's averaged value $\langle \Psi \rangle^2$,
(iii) $\frac{4}{3\pi}M$ obtained from the total mass,
(iv) the squared minimum of the conformal $\Psi_{\min}^2$.

The results for the first eight iterations of the pentatope-based Apollonian configurations are shown in figure 9. All values are given in units of the size a_0 of the swiss-cheese dust universe. Hence, the best fit should approach the value 1. However, we observe that the values differ from each other substantially and none really approaches the dust universe size; although the unifoamy size (6) and the squared minimum (6) seem to approach this value, they actually miss it. Furthermore, our suggestion (6) differs strongly from the averaged value (6) but it is closer to the squared minimum. Note that Korzyński's first theorem would give almost the same (large) upper bounds for the deviation from the minimum because the spherical cap discrepancy should not really differ for the different iterations because we keep the biggest caps. For unifoamy configurations, our suggestion should be close to the size (6) derived from the total mass, but this is not the case. Actually, if we check the unifoamy conditions (70) for all masses, we notice that they are violated by the biggest masses. Besides the spherical cap discrepancy, this indicates that very big masses are not possible for Friedmann-like configurations. This is consistent with our expectation that the masses in Friedmann-like configurations should be distributed somehow uniformly. In the considered configurations, the five biggest masses contained about half of the total mass.
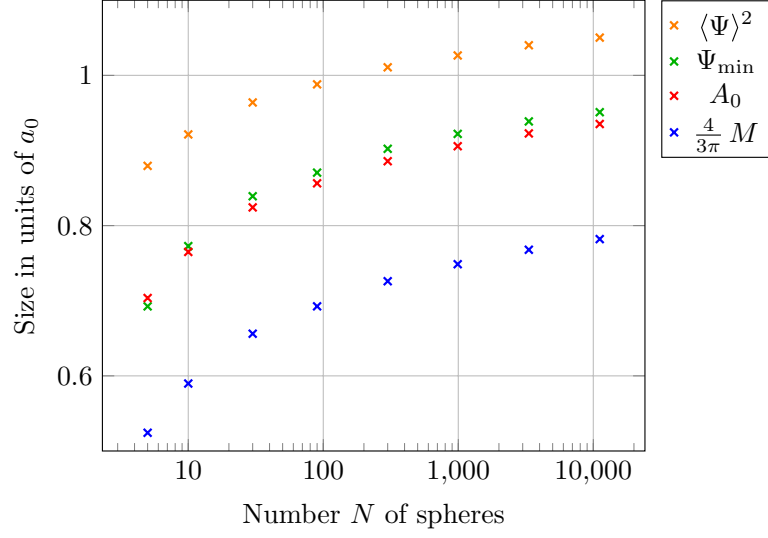
Figure 9. Comparison between the different fits for the initial data with a swiss-cheese universe with size a_0. In both cases, the configuration is given by the Apollonian packing discussed above such that the black-holes are located at the same positions with the same masses.
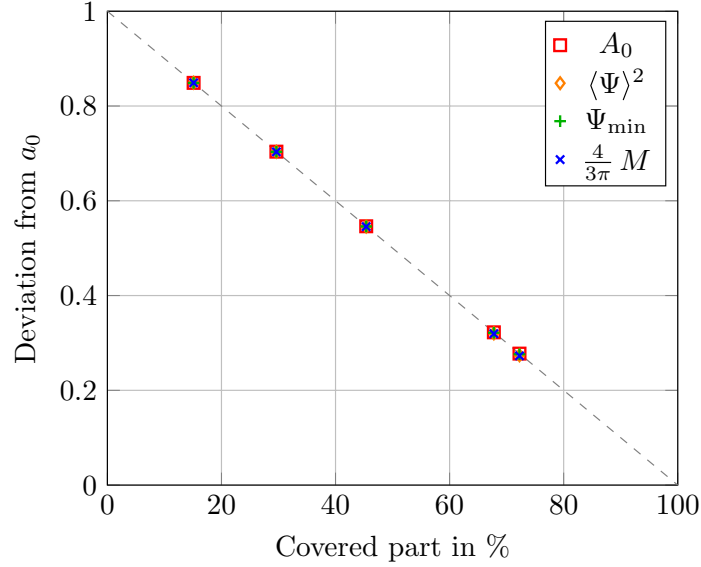

Figure 10. Modified Apollonian configurations such that the biggest masses are replaced by smaller black-holes. All five configurations contain about 12 000 black-holes.

In order to achieve a more uniform configuration, we substitute the biggest spheres by smaller ones, using the method described at the end of section 2. We recall that this means, first of all, to pick a Descartes set within each largest sphere, which we again choose to be that of a regular pentatope, i.e. spheres of equal size. (We recall that any other choice would

be related to this one by a Lorentz transformation.) Based on that choice, we can now continue the Apollonian packing to the inside of each largest sphere, so as to reduce the largest sphere-size to that of the largest ones inside those that formerly had been the largest ones. This step can be iterated, in our case by always sticking to the equal-size (i.e. pentatope-based) Descartes set, until the size of the maximal spheres falls below a given upper bound. In figure 10 we have plotted the deviation from the size of the swiss-cheese dust universe for five configurations obtained from the pentatope-based Apollonian configurations with different maximal sizes for the spherical caps, as just described.

In order to reduce the computational effort (which is entirely due to the quadratic equation (54) for the μ_i) we have also removed the smallest caps so that we h ave about 10^5 masses in all five cases. This time, the configurations are approximately unifoamy and therefore the different results are in good agreement with each other. However, we also observe that the deviation from the swiss-cheese value is often quite large. But if we check how much of the dust universe in the swiss-cheese model is removed, we observe that the fit becomes better the less dust is remaining, which clearly fits expectation. In fact, the deviation appears to be proportional to the amount of remaining dust or, equivalently, the volume to the part of the 3-sphere that is uncovered by spherical caps. We conclude that the unifoamity of a configuration is not sufficient to guarantee a good fit, we also need an effective covering of the 3-sphere in the sense just explained.

The number of black-holes in our computations is mainly limited by numerical reasons in calculating the mass parameters. We mention that the mass parameters can be estimated by

$$\mu_i \approx m_i \sqrt{\frac{3\pi}{16M}} \tag{77}$$

for unifoamy configurations, so that this step may be skipped leading to small deviations between the masses of the swiss-model and the initial data. Furthermore, it is also possible to use the masses m_i instead of the mass parameters μ_i in order to check if a given configuration is unifoamy. This is true because it can be shown that

$$\frac{\mu_i}{\mu} \approx \frac{m_i}{M}. \tag{78}$$

This ends our first small excursion into applications of Lie sphere geometry to lattice cosmology. We hope to have convinced the reader that this is not only a beautiful but also very powerful method for the systematic construction of black-hole configurations of almost arbitrary degrees of symmetry. We regard this paper only as a first step in this direction, the primary purpose of which is to introduce the method and explain its geometric foundations. We are convinced that a proper geometric understanding is essential in order to bring this method to its full power. Further work will be devoted to more concrete applications.

Acknowledgments

Appendix A. Solution of Lichnerowicz equation on S^3

In this appendix we give a simple and general argument that implies that (53) solves (52). This fact is a special case of the following general

Theorem. Let Δ_{S^n} denote the Laplacian on the unit n-sphere which we think of as being embedded into $(n+1)$—dimensional Euclidean space: $S^n := \{x \in \mathbb{R}^{n+1} : \|x\| = 1\}$. Let E denote an arbitrary element of S^n, locally parametrised by some n coordinates, like generalised polar angles, and $P \in S^n$ a fixed point. We define the strictly positive function $D : S^n - \{P\} \to \mathbb{R}$, $D(E) := \|E - P\|$ which associates with each $E \in S^n - \{P\}$ its distance to P along the straight in $\mathbb{R}^{n+1}$. In other words: $D(E)$ denotes the geodesic distance of E from P as measured in the embedding $\mathbb{R}^{n+1}$, *not* the intrinsic geodesic distance in S^n (which is obviously always strictly larger). Then the theorem states that $D^{-(n-2)}$ is an eigenfunction of the Laplacian on $S^n - P$ with eigenvalue $n(n-2)/4$:

$$\Delta_{S^n} D^{-(n-2)} = \frac{n(n-2)}{4} \cdot D^{-(n-2)}. \tag{A.1}$$

In particular, for $n = 3$ we get $\Delta_{S^3} D^{-1} = \frac{3}{4} \cdot D^{-1}$, which is just the statement that (53) solves (52).

Proof. Consider the function $\tilde{D} : \mathbb{R}^{n+1} \to \mathbb{R}$, $\tilde{D}(rE) := \|rE - P\|$, where rE denotes a general point in $\mathbb{R}^{n+1} - \{0\}$ whose norm is just $r > 0$. The function $\tilde{D} =$ just extends D, i.e. $\tilde{D}\big|_{S^n} = D$. Now, the Laplacian on $\mathbb{R}^{n+1}$ can be written as follows:

$$\Delta_{\mathbb{R}^{n+1}} = \partial_r^2 + \frac{n}{r}\partial_r + r^{-2}\Delta_{S^n}. \tag{A.2}$$

This formula allows us to calculate the Laplacian of any real-valued function F on (an open subset of) S^n by means of the Laplacian of any extension $\tilde{F}$ of it to $\mathbb{R}^{n+1}$ (which is much easier to compute) and further simple r-differentiations. The formula we are using is:

$$\Delta_{S^n} F = \left(\Delta_{\mathbb{R}^{n+1}} - \partial_r^2 - \frac{n}{r}\partial_r\right)\bigg|_{r=1} \tilde{F}. \tag{A.3}$$

In our case we have $\tilde{D}(rE) = (r^2 - 2rf + 1)^{1/2}$, where $f := E \cdot P$ is a real valued function on S^n, independent of r. Simple calculations now show that

$$\tilde{D}_1 = D = \sqrt{2(1-f)}, \quad \tilde{D}_1' = \frac{1}{2}D, \quad \tilde{D}_1'' = -\frac{1}{4}D + \frac{1}{D}, \tag{A.4}$$

where a prime denotes differentiation with respect to r and the subscript 1 indicates the restriction of the respective function (after differentiation) to S^n, i.e. $r = 1$.

Now we take $\tilde{F} = \tilde{D}^{-k}$. The Laplacian of that in $\mathbb{R}^{n+1}$ is very easy to calculate, e.g. by using spherical polar coordinates based at P, in which case, using ρ as radial coordinate, we have $\tilde{D}(E) = \rho$ and $\Delta_{\mathbb{R}^{n+1}} = \partial_\rho^2 + (n/\rho)\partial_\rho$, so that

$$\Delta_{\mathbb{R}^{n+1}}\bigg|_{r=1} \tilde{D}^{-k} = k(k+1-n)D^{-k-2}. \tag{A.5}$$

Furthermore, using (A.4) a short computation shows

$$\left(\partial_r^2 + (n/r)\partial_r\right)\bigg|_{r=1} \tilde{D}^{-k} = -k D^{-k-2} + \frac{k}{4}\left(k - 2n + 2\right)D^{-k}. \tag{A.6}$$

Hence (A.3) applied to $F = D^{-k}$ gives

$$\Delta_{S^n} D^{-k} = k(k + 2 - n) D^{-k-2} + \frac{k}{4}(2n - k - 2) D^{-k}. \tag{A.7}$$

If we choose $k = n - 2$ the first term vanishes and $D^{-k} = D^{2-n}$ becomes an (unbounded) eigenfunction of Δ_{S^n} on $S^n - \{\boldsymbol{P}\}$ with eigenvalue $n(n-2)/4$, as stated in (A.1). $\qquad\square$

Appendix B. Stereographic projection and its metric properties

In this appendix we recall some properties of the stereographic projection from the unit n-sphere in $\mathbb{R}^{(n+1)}$ (or any Euclidean vector space of that dimension) onto its equatorial plane and the relation between the Euclidean distances of source- and image points.

We consider $\mathbb{R}^{(n+1)}$ with the usual Euclidean inner product and norm. As before, the latter will be denoted by $\|\cdot\|$. Again we consider the embedded unit n-sphere $S^n := \{\boldsymbol{X} \in \mathbb{R}^{(n+1)} : \|\boldsymbol{X}\| = 1\}$. Points in $\mathbb{R}^{(n+1)}$ which lie on S^n are denoted by capital bold-faced letters, like $\boldsymbol{X}, \boldsymbol{Y}$, etc. Their inner product, according to the Euclidean structure in $\mathbb{R}^{(n+1)}$, will be denoted by a dot, like $\boldsymbol{X} \cdot \boldsymbol{Y}$; hence, e.g. $\boldsymbol{X}^2 := \boldsymbol{X} \cdot \boldsymbol{X} = \|\boldsymbol{X}\|^2$.

We select a point $\boldsymbol{P} \in S^3$, called the 'pole', which will serve us as centre of the stereographic projection. Further, we let $\boldsymbol{P}^\perp := \{\boldsymbol{X} \in \mathbb{R}^{(n+1)} : \boldsymbol{X} \cdot \boldsymbol{P} = 0\} \simeq \mathbb{R}^n$ be the 'equatorial plane' (a linear subspace), elements of which we denote by lower case bold-faced letters, like $\boldsymbol{x}, \boldsymbol{y}$. The subspace $\boldsymbol{P}^\perp$ inherits a Euclidean structure and norm from $\mathbb{R}^{(n+1)}$, which we continue to denote by a dot and $\|\cdot\|$, respectively.

The given data define a diffeomorphism $\pi : S^n - \{\boldsymbol{P}\} \to \boldsymbol{P}^\perp$. It is called the stereographic projection from the pole onto the equatorial plane and is given by assigning to any $\boldsymbol{X} \in S^n - \{\boldsymbol{P}\}$ the unique intersection point of the line through $\boldsymbol{X}$ and $\boldsymbol{P}$ with $\boldsymbol{P}^\perp$. The parametric form (parameter $\lambda \in \mathbb{R}$) of the line is given by $\boldsymbol{L}(\lambda) = \boldsymbol{S} + \lambda(\boldsymbol{X} - \boldsymbol{P})$ and its intersection with $\boldsymbol{P}^\perp$ by $\boldsymbol{L}(\lambda_*)$, where λ_* follows from $\boldsymbol{L}(\lambda_*) \cdot \boldsymbol{P} = 0$. This gives

$$\boldsymbol{x} := \pi(\boldsymbol{X}) = \frac{\boldsymbol{X} - \boldsymbol{P}(\boldsymbol{P} \cdot \boldsymbol{X})}{1 - \boldsymbol{P} \cdot \boldsymbol{X}}. \tag{B.1}$$

Its inverse is given by

$$\boldsymbol{X} = \pi^{-1}(\boldsymbol{x}) = \boldsymbol{x}\,\frac{2}{\boldsymbol{x}^2 + 1} + \boldsymbol{P}\,\frac{\boldsymbol{x}^2 - 1}{\boldsymbol{x}^2 + 1}. \tag{B.2}$$

Equations (B.1) and (B.2) define the stereographic diffeomorphism between the once-punctured n-sphere and the equatorial n-plane.

Next we wish to relate the Euclidean distances between source- and image points. We start by noting that

$$\|\boldsymbol{X} - \boldsymbol{P}\|^2 = 2(1 - \boldsymbol{X} \cdot \boldsymbol{P}) = \frac{4}{1 + \boldsymbol{x}^2}, \tag{B.3}$$

where we used $\boldsymbol{X}^2 = \boldsymbol{P}^2 = 1$ and (B.2) with $\boldsymbol{x} \cdot \boldsymbol{P} = 0$ in the 2nd step. Similarly, for $\boldsymbol{X} := \pi^{-1}(\boldsymbol{x})$ and $\boldsymbol{Y} := \pi^{-1}(\boldsymbol{y})$, equation (B.2) yields

$$\boldsymbol{X} \cdot \boldsymbol{Y} = \frac{4\,\boldsymbol{x} \cdot \boldsymbol{y} + (\boldsymbol{x}^2 - 1)(\boldsymbol{y}^2 - 1)}{(\boldsymbol{x}^2 + 1)(\boldsymbol{y}^2 + 1)}, \tag{B.4}$$

and hence

$$4\,\|X-Y\|^2 = 8(1-X\cdot Y) = \frac{16(x-y)^2}{(1+x^2)(1+y^2)}$$
$$= \|x-y\|^2\,\|X-P\|^2\,\|Y-P\|^2, \tag{B.5}$$

using (B.3) for X and Y in the last step. This leads to the final relation

$$\|x-y\| = \frac{2\,\|X-Y\|}{\|X-P\|\,\|Y-P\|} \tag{B.6}$$

that holds independently of the dimensions n and that we used in (59).

The Riemannian metric of S^n is that induced by the embedding $S^n \hookrightarrow \mathbb{R}^{(n+1)}$. In stereographic coordinates $x \in P^\perp$ this metric follows from pulling back the Riemannian metric on S^n via the inverse stereographic projection π^{-1}. This is easily computed from (B.2) by first calculating the differential of $X(x)$,

$$\mathbf{d}X = \frac{2}{1+x^2}\,\mathbf{d}x + \frac{4\,(P-x)}{(x^2+1)^2}\,(x\cdot\mathbf{d}x), \tag{B.7}$$

and then 'squaring' it, $\mathbf{d}X\dot{\otimes}\mathbf{d}X := \delta_{ab}\mathbf{d}X^a \otimes \mathbf{d}X^b$, which immediately gives, taking into account $x\cdot P = 0$ and $\mathbf{d}x\cdot P = 0$,

$$\mathbf{d}X\dot{\otimes}\mathbf{d}X == \left(\frac{2}{1+x^2}\right)^2\,\mathbf{d}x\dot{\otimes}\mathbf{d}x. \tag{B.8}$$

Comparison with (B.3) shows that the flat metric $h_{\mathbb{R}^n} := \mathbf{d}x\cdot\mathbf{d}x$ on $P^\perp \cong \mathbb{R}^n$ can be written in terms of the constant positive-curvature metric on the unit n-sphere, $h_{S^n} := (\pi^{-1})^*(\mathbf{d}X\cdot\mathbf{d}X)$, as follows:

$$h_{\mathbb{R}^n} = \frac{4}{\|X-P\|^4}\,h_{S^n}. \tag{B.9}$$

This is the equation we used in (57).

ORCID iDs

Domenico Giulini https://orcid.org/0000-0003-3123-7257

References

[1] Bartnik R 1986 The mass of an asymptotically flat manifold *Commun. Pure Appl. Math.* **39** 661–93
[2] Battye R A, Gibbons G W and Sutcliffe P M 2003 Central configurations in three dimensions *Proc. R. Soc.* A **459** 911–43
[3] Baumgarte T W and Shapiro S L 2010 *Numerical Relativity: Solving Einstein's Equations on the Computer* (Cambridge: Cambridge University Press)
[4] Bentivegna E and Korzyński M 2012 Evolution of a periodic eight-black-hole lattice in numerical relativity *Class. Quantum Grav.* **29** 165007
[5] Bentivegna E, Clifton T, Durk J, Korzyński M and Rosquist K 2018 Black-hole lattices as cosmological models *Class. Quantum Grav.* **35** 175004
[6] Bentivegna E, Korzyski M, Hinder I and Gerlicher D 2017 Light propagation through black-hole lattices *J. Cosmol. Astropart. Phys.* JCAP17(2017)014
[7] Borkovec M, De Paris W and Peikert R 1994 The fractal dimension of the apollonian sphere packing *Fractals* **02** 521–6

[8] Brightwell G and Winkler P 1989 Sphere orders *Order* **6** 235–40

[9] Brill D R and Lindquist R W 1963 Interaction energy in geometrostatics *Phys. Rev.* **131** 471–6

[10] Buchert T 2011 Toward physical cosmology: focus on inhomogeneous geometry and its non-perturbative effects *Class. Quantum Grav.* **28** 164007

[11] Buchert T *et al* 2015 Is there proof that backreaction of inhomogeneities is irrelevant in cosmology? *Class. Quantum Grav.* **32** 215021

[12] Carrera M and Giulini D 2010 Influence of global cosmological expansion on local dynamics and kinematics *Rev. Mod. Phys.* **82** 169–208

[13] Cecil T E 1992 *Lie Sphere Geometry* (Berlin: Springer)

[14] Clarkson C, Ellis G, Larena J and Umeh O 2011 Does the growth of structure affect our dynamical models of the universe? The averaging, backreaction, and fitting problems in cosmology *Rep. Prog. Phys.* **74** 112901

[15] Clifton T 2013 Back reaction in relativistic cosmology *Int. J. Mod. Phys.* D **22** 1330004

[16] Clifton T, Gregoris D, Rosquist K and Tavakol R 2013 Exact evolution of discrete relativistic cosmological models *J. Cosmol. Astropart. Phys.* JCAP13(2013)010

[17] Clifton T, Rosquist K and Tavakol R 2012 An exact quantification of backreaction in relativistic cosmology *Phys. Rev.* D **86** 043506

[18] Druk J and Clifton T 2017 A quasi-static approach to structure formation in black hole universes *J. Cosmol. Astropart. Phys.* JCAP10(2017)012

[19] Durk J and Clifton T 2017 Exact initial data for black hole universes with a cosmological constant *Class. Quantum Grav.* **34** 065009

[20] Einstein A and Straus E G 1945 The influence of the expansion of space on the gravitation fields surrounding the individual stars *Rev. Mod. Phys.* **17** 120–4

[21] Ellis G F and Gibbons G W 2014 Discrete Newtonian cosmology *Class. Quantum Grav.* **31** 025003

[22] Fennen M 2017 Multi-black-hole configurations as models for inhomogeneous cosmologies *PhD Thesis* University of Bremen

[23] Freudenthal H 1931 Über die Enden topologischer Räume und Gruppen *Math. Z.* **33** 692–713

[24] Gibbons G W and Werner M C 2013 On de Sitter geometry in crater statistics *Mon. Not. R. Astron. Soc.* **429** 1045–50

[25] Gibbons G W, Werner M C, Yoshida N and Chon S 2014 On de Sitter geometry in cosmic void statistics *Mon. Not. R. Astron. Soc.* **438** 1603–10

[26] Dynamical G D 2014 Hamiltonian formulation of general relativity *Springer Handbook of Spacetime* ed A Ashtekar and V Petkov (Berlin: Springer) pp 323–62 (Extended version (76 pages) at arXiv:1505.01403)

[27] Gosset T 1937 The Hexlet *Nature* **139** 251–2

[28] Graham R L, Lagarias J C, Mallows C L, Wilks A R and Yan C H 2005 Apollonian circle packings: geometry and group theory I. The Apollonian group *Discrete Comput. Geom.* **34** 547–85

[29] Graham R L, Lagarias J C, Mallows C L, Wilks A R and Yan C H 2006 Apollonian circle packings: geometry and group theory II. Super-Apollonian group and integral packings *Discrete Comput. Geom.* **35** 1–36

[30] Graham R L, Lagarias J C, Mallows C L, Wilks A R and Yan C H 2006 Apollonian circle packings: geometry and group theory III. Higher dimensions *Discrete Comput. Geom.* **35** 37–72

[31] Israel W 1966 Singular hypersurfaces and thin shells in general relativity *Il Nuovo Cimento* B **44** 1–14

[32] Korzyński M 2014 Backreaction and continuum limit in a closed universe filled with black holes *Class. Quantum Grav.* **31** 085002

[33] Korzyński M 2015 Nonlinear effects of general relativity from multiscale structure *Class. Quantum Grav.* **32** 215013

[34] Korzyński M, Hinder I and Bentivegna E 2015 On the vacuum Einstein equations along curves with a discrete local rotation and reflection symmetry *J. Cosmol. Astropart. Phys.* JCAP15(2015)025

[35] Lagarias J C, Mallows C L and Wilks A R 2002 Beyond the descartes circle theorem *Am. Math. Mon.* **109** 338–61

[36] Lie S 1872 Ueber Complexe, insbesondere Linien- und Kugel-Complexe, mit Anwendung auf die Theorie partieller Differential-Gleichungen *Math. Ann.* **5** 145–208

[37] Lindquist R W and Wheeler J A 1957 Dynamics of a lattice universe by the Schwarzschild-cell method *Rev. Mod. Phys.* **29** 432–43

[38] Liu R G 2015 Lindquist–Wheeler formulation of lattice universes *Phys. Rev.* D **92** 063529

[39] Soddy F 1936 The Kiss precise *Nature* **137** 1021

[40] Söderberg B 1992 Apollonian tiling, the Lorentz group, and regular trees *Phys. Rev.* A **46** 1859–66